Nanomaterials for Sustainable Water Remediation

Sheila M. Goodman

A thesis

Submitted in partial fulfillment of the

Requirements for the degree of

Master of Science

University of Washington

2018

Committee:

Anthony Dichiara, chair

Fernando Resende

Renata Bura

Program Authorized to Offer Degree:

Environmental and Forest Science

University of Washington

Abstract

Nanomaterials for Sustainable Water Remediation

Sheila M. Goodman

Chair of the Supervisory Committee:
Dr. Anthony Dichiara
Bioresource Science and Engineering

Ever increasing industrialization leads to a rise in contaminated water resources due to the release of pollutants, such as organic dyes, into aquatic environments. Adsorption process, which involves the transfer of undesirable chemicals from a fluid phase to the surface of a solid adsorbent with high binding affinity and capacity, has become a leading separation technique for point-of-use water applications. Due to their high surface area, nanomaterials, such as carbon nanotubes or graphene, have the ability to uptake larger amounts of molecules before reaching saturation than conventional adsorbents like biochar. However, nanomaterials have the tendency to aggregate, hindering their adsorption properties and causing detrimental pressure drops in continuous flow systems. To avoid this, carbon nanomaterials can be dispersed using surfactants and deposited into porous templates. In this research, we propose using lignin in tandem with a double-acoustic irradiation system as a sustainable surfactant and hardwoods as renewable supports for nanosorbents to prevent material agglomeration and facilitate fast water transport. Hardwoods exhibit a unique mesoporous structure, comprising partially aligned, hollow channels (vessels), connected together through perforation plates with micrometer-sized pores, enabling

continuous conduction of fluids along the wood channels. Here, we prepared sustainable water filters by decorating the hardwood template with aqueous solutions of alkali lignin and graphene nanoplatelets using a vacuum assisted impregnation method for the removal of methylene blue from aqueous solutions. Results showed that complete removal of methylene blue was achieved within a broad range of concentrations even at high flow rates, providing great opportunities for environmental remediation and separation applications.

TABLE OF CONTENTS

LIST OF FIGURES

LIST OF TABLES

INTRODUCTION

Fresh water is essential for all life on earth, and is a crucial feedstock for the majority of agricultural and industrial processes. The demand for fresh water is ever increasing due to increasing population, but availability is decreasing due to the resulting rise in environmental pollution from industrialization.[1,2,3] Contaminated environmental systems and groundwater is further reducing the available fresh water for human and animal consumption. The most prevalent contaminants include organic dyes, pharmaceuticals, personal care products (PCPs), pesticides, and metal oxides.[4,5,6] All of these contaminants are known to have adverse effects on aquatic environments as well as human health due to their toxic, carcinogenic, and slow degradation rate effects.

Recent efforts have been made to limit the amount of waste being released to environmental systems and to develop innovative removal techniques to help preserve aquatic environments and fresh water supplies. Many techniques include physical or chemical adsorption, membrane filtration, and photocatalytic degradation.[7,8,9,10] While effective at removing desired contaminants from aqueous systems, the need for an effective, simple, and inexpensive water treatment technique still poses a significant need. Adsorption, which involves the transfer of undesirable compounds from a fluid phase to the surface of a solid adsorbent with high binding affinity and capacity, has become a leading separation technique for point-of-use water applications.[11] One major problem concerning adsorption techniques is the accumulation of contaminants in a solid adsorbent. In an effort to mitigate this concern, increased emphasis has been placed on the use of bio-based adsorbents as a sustainable alternative to limit the amount of accumulated waste, including bio-char, cellulosic based materials, and activated carbon produced from forest and agricultural residue.[12,13] However, a significant amount of chemical pretreatment is necessary to

ensure bio-based adsorbents are modified to promote optimal adsorption of desired compounds, increasing processing time and costs.

Carbon nanomaterials, such as carbon nanotubes (CNTs) and graphene, have also gained support as adsorbents in the last few years due to their large available surface area, allowing for the ability to uptake larger amounts of molecules before reaching saturation than conventional bio-based adsorbents such as bio-char. However, the hydrophobicity of carbon nanomaterials and their tendency to readily form aggregates due to strong van der Waals forces, significantly hampers the properties of carbon nanomaterial-based products and limits the surface area available for adsorption, as well as causing detrimental pressure drops in continuous flow systems.[14,15] Hence, the individualization of carbon nanomaterial aggregates is necessary to take full advantage of the potential of all carbon nanomaterials. Various techniques to disperse carbon nanomaterials have been developed, including high shear mixing, sonication, and ultracentrifugation.[16] These methods can be divided into two different categories depending on the nature of the surface modification used to improve the dispersion of carbon nanomaterials. On one hand, covalent functionalization aims at disrupting the stacking properties of carbon nanomaterials by grafting functional groups on the surface to alter the hydrogen bonding and intercalate chemical species between the aggregates.[17] On the other hand, noncovalent functionalization involves the physical adsorption of surfactants, polymers, DNA, and peptides.[18,19,20,21] The noncovalent bonding of surfactants with carbon nanomaterials is typically considered as a superior approach since it does not modify the π-electron network and preserves the structural integrity. In addition, surfactants can be relatively easily removed after treatment by washing. A large variety of surfactants, such as sodium dodecyl-benzenesulphonate (SDBS),[22] octyl phenol ethoxylate (Triton X-100),[23] cetyltrimethylammonium bromide (CTAB),[24] and sodium dodecyl sulfate (SDS)[18,25] have been examined for the dispersion

of carbon nanomaterials in aqueous solutions under the noncovalent approach. However, the great majority of surfactants are petroleum-based chemicals. As environmental concerns rise and oil prices continue to trend upward due to diminishing supply, a greater emphasis on renewable resources is needed to explore new classes of dispersants to prepare carbon nanomaterial solutions. Another, less common way to minimalize the agglomeration of carbon nanomaterials and preserve their high surface area involves depositing nanomaterials into porous templates. Hardwoods exhibit a unique mesoporous structure, comprising partially aligned, hollow channels (vessels), connected together through perforation plates with micrometer-sized pores, enabling continuous conduction of fluids along the wood channels.[26] Here, we propose using hardwoods as renewable supports for nanosorbents such as graphene nanoplatelets (GnPs) to prevent material agglomeration and facilitate bulk water treatment in a continuous adsorption study.

CHAPTER 1: Lignin-assisted double acoustic irradiation for concentrated aqueous dispersions of carbon nanotubes

Lignin is the second most abundant natural polymer and represents up to 30% of the world organic biomass. Despite its widespread availability, the applications of lignin are rather limited. Currently, lignin is an underutilized byproduct of the pulp and paper industry and often treated as a waste that is burned for energy recovery. Lignin was discovered in 1838 by Anselme Payen and consists of a three-dimensional, highly cross-linked, phenylpropane-type macromolecule mainly comprised of carbon and oxygen with no structural regularity within its polymeric framework.[27] Due to its amphiphilic nature and the possibility of π-π interactions with graphitic structures, opportunities exist to use lignin as a renewable dispersing agent for the preparation of aqueous solutions of carbon nanomaterials. While lignin was recently found to promote the debundling of

CNTs in water,[28,29] no comparative assessment of the dispersion quality achieved using lignin and other typical petroleum-based surfactants under identical experimental conditions has been reported to date.

The present research provides a benchmark of the effectiveness of lignin in dispersing CNTs. Aqueous suspensions of multiwalled CNTs are examined using alkali lignin (AL), SDS, and CTAB. UV-vis spectroscopy and optical microscopy are employed to assess the dispersion state and stability of CNTs in water. The influence of sonication energy, dispersant concentration, CNT morphology and oxidation are analyzed. Acoustic irradiation using an innovative system combining both bath and probe sonication is also studied. Finally, binary and ternary mixtures of different mixing ratios of AL/SDS, AL/CTAB, and AL/SDS/CTAB are prepared to investigate possible synergistic effects that can improve surfactant adsorption on CNT surfaces and modifications of repulsive/attractive forces. This research provides relevant new insights to optimize CNT dispersions using renewable bio-based compounds which can be applied to a variety of other carbon nanomaterials. This work has already been published in RSC Advances in 2017.[30]

Experimental Methods

Materials

Pristine and hydroxyl-functionalized CNTs with length of 10-20 μm and outer diameters below 8 nm and above 50 nm synthesized by catalytic chemical vapor deposition and purified using acid chemistry were purchased from Cheap Tubes Inc. The hydroxyl-functionalized CNTs per the manufacturer technical data contain 5.5% of OH groups. The main characteristics of the CNTs used in this study, including length, inner and outer diameter, and specific surface area are summarized in **Table 1**. All CNTs were used as received without any further treatment. The alkali lignin (AL, 99%), sodium dodecyl sulfate (SDS, 99%) and cetyltrimethylammonium bromide

(CTAB, 99%) dispersants were obtained from Tokyo Chemical Industry Co., MP Biomedicals, and Amresco, respectively. All dispersions were conducted using de-ionized (DI) water.

Table 1. Length, inner/outer diameter, and surface area of the various CNTs used in this work.

Sample	Length (μm)	Inner diameter (nm)	Outer diameter (nm)	Specific surface area (m^2/g)
8-CNT	10-20	2-5	<8	500
50-CNT	10-20	5-10	50-80	60
8-CNT-OH	10-20	2-5	<8	500
50-CNT-OH	10-20	5-10	50-80	60

Method

A desired amount of dispersant was added to DI water to compare the dispersive efficiency of AL, SDS, and CTAB. Once the dispersant was completely dissolved after 10 minutes of bath sonication at room temperature (25ºC), CNTs were added into the solutions at a constant concentration of 1 wt% (CNT powder weight per water weight), which is more concentrated than typical suspensions of CNTs reported in the literature.[31] The solution pH was kept at the natural level in all experiments (i.e. pH~7). CNTs with different outer diameters (8 and 50 nm) and functional groups (pristine and OH-functionalized) were examined. For mixed dispersant systems, binary and ternary mixtures of different mixing ratios of AL/SDS, AL/CTAB, and AL/SDS/CTAB were prepared under similar conditions. Unless otherwise specified, all CNTs dispersions were sonicated in an ice bath for 30 minutes using a 750 W Sonics Vibracell VCX probe sonicator equipped with a 13 mm stepped tip and running at 20% of maximum amplitude. The as-sonicated samples were then centrifuged at 5,000 rpm for 30 minutes to remove large undispersed clusters. The supernatants were diluted appropriately and probe sonicated for an additional 15 minutes at 20% amplitude for further

comparative analysis by UV-vis absorption spectroscopy. To study the colloidal stability of the different CNT dispersions, the samples were stored at room temperature, in the dark, without agitation, and periodical measurements were taken over a 34 day time period.

Characterization

UV-vis measurements were performed in quartz cuvettes at room temperature (25ºC) using a Perkin Elmer Lambda 750 spectrophotometer operating in the 300-1200 nm range. The blanks were obtained using the original dispersant solutions diluted by the same factor and under the same conditions as the samples themselves. Indirect optical observations of the CNT dispersions were achieved by drop casting the different suspensions onto glass slides for observation using a Zeiss Axiocam ERc5s digital camera mounted on a Zeiss Axiolab light microscope. Direct imaging was conducted using a wet transmission electron microscopy (TEM) technique to assess the dispersion state of CNTs in suspensions. Unlike conventional TEM, the wet TEM method can overcome the inherent limitations induced by drying and exposing the sample to vacuum before imaging, hence allowing for representative *in-situ* images of the dispersions to be taken without altering the original conditions of the fluid. The wet-cell was constructed by holding the solution between two silicon nitride membrane window TEM grids, and observed using a FEI TECNAI G2 F20 S-TWIN high resolution TEM with a beam acceleration voltage of 200 keV.

Results and discussion

Influence of dispersant concentration

UV−vis spectroscopy is one of the most commonly used techniques to evaluate the quality of CNT dispersions.[32] It involves the quantification of the portion of light absorbed as it travels through the CNT suspension, relative to its blank counterpart. Individual disentangled CNTs are active in the UV−vis region and display characteristic bands corresponding to absorption due to 1D Van

Hove singularities.[33] However, the photoluminescence that is normally detected by UV–vis spectroscopy is quenched in bundled CNTs, meaning that CNT aggregates hardly absorb light in the wavelength range between 300 and 1200 nm.[34] Based on this principle, the degree of individualization of CNTs in aqueous solution can be related to the intensity of the corresponding absorption spectrum.[35] For comparison purposes, the UV-vis spectra of aqueous CNT dispersions using different AL, SDS and CTAB concentrations are recorded, as illustrated in **Figure 1**. Representative photographs of sonicated CNT aqueous suspensions with the different dispersants are shown in the insets (**Fig. 1a-c**) and reveal the Tyndall effect, which is indicative of colloidal systems.[36] In each case, the absorbance in the UV-vis region rises with the addition of dispersant as compared to CNT suspensions prepared without any surfactant. In particular, it can be observed that the absorbance intensity increases with the dispersant concentration up to a certain level beyond which a further increase in concentration leads to a reduction of the absorbance intensity. The optimal dispersant concentrations yielding the highest absorbance under the considered conditions are determined to be 2 wt% for both AL, SDS and CTAB, which is higher than their critical micelle concentrations (6mM for SDS and 0.8 mM for CTAB). Further increase of AL, SDS and CTAB concentrations above these optimal values not only represents a waste of dispersants but also induces undesired effects. This is consistent with other studies reporting the aqueous dispersion of CNTs using various surfactants.[37,38]

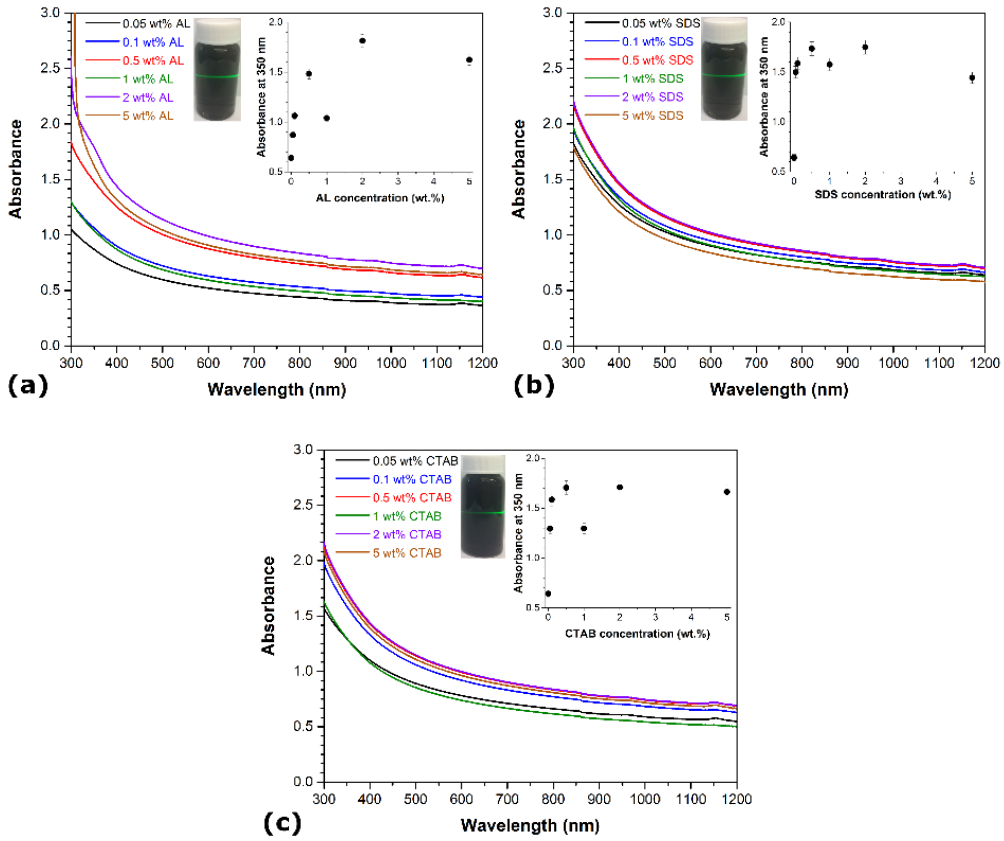

Figure 1. UV-vis spectra of aqueous CNT suspensions (1 wt%) using different dispersant concentrations of (a) AL, (b) SDS, and (c) CTAB. Graphs of absorbance at 350 nm as a function of dispersant concentration and representative photographs of the CNT dispersions are shown in insets.

The well-accepted "unzippering" mechanism can be employed to describe the dispersion of CNTs in aqueous solutions.[39] Ultrasonication provides a high local shear at the CNT bundle end caused by cavitation. Cavitation occurs during the rarefaction sequence of an applied sonication wave, which causes the formation of solvent cavities or vacuum bubbles when the solution pressure drops below ambient.[40] These expanding gas pockets collapse due to escalating stresses in their walls, releasing large amounts of energy in the form of high local pressure and temperature, and resulting

in liquid jets of up to 280 m/s velocity. This phenomenon generates gaps between CNT bundles, where dispersant molecules can enter to adsorb onto the newly available CNT surface, hence keeping the connected CNTs partially separated. As the partially individualized CNTs move relative to the bundle due to Brownian motion, the dispersant coating continues to propagate along the CNT length until a complete separation occurs. Suspended single CNTs are considered stable when the interaction between the dispersant and CNT is strong enough to overcome the van der Waals force and π–π interactions between neighboring CNTs. Depending on the nature of the dispersant, electrostatic repulsion and/or steric hindrance prevent the dispersant-CNT complexes from sticking together. As a result, an equilibrium is reached between single nanotubes and bundles, which varies with concentration. At low concentrations, the dispersant adsorption is limited and does not efficiently counterbalance the van der Waals-induced aggregation of CNTs. However, when the amount of dispersant in the aqueous solution is above a certain value, large micelles form around the CNT bundles and exert an osmotic pressure creating a depletion-induced attraction.[41] Under similar conditions (i.e. concentration, sonication, temperature…), the variations in dispersion efficiency between different surfactants is closely related to their interaction with CNTs, which depends on the length of their alkyl chain, the presence of benzene rings, and the type of head group.[42] At the optimal concentrations, the degree of individualized CNTs in water is comparable among the different dispersions, with a slight increase in the order of AL>CTAB>SDS, as indicated by their respective absorbance values. While hydrogen bonding can form between hydroxyl groups on AL and polar groups on the CNT surfaces, the adsorption of AL is mostly attributed to the presence of a large number of condensed aromatic structures promoting π–π interactions with CNTs.[36,43] The dispersion of CNTs is known to be positively correlated with the number of aromatic rings in the surfactants. Without aromatic units, the uptake of SDS and

CTAB on CNTs, which involves relatively weaker hydrophobic interactions, is expected to be lower than that of AL.

Influence of sonication type and energy

The onset and intensity of cavitation, which is influenced by various factors including the viscosity of the solution and sonication energy, plays a critical role in the dispersion dynamics of CNTs in solution.[44] **Figure 2** describes the evolution of absorbance for the different aqueous CNT suspensions as a function of the total energy supplied to the solution. In all experiments, the sonication amplitude is kept constant at 28% and the amount of sonication energy is varied by adjusting the processing time. Comparing the UV-vis spectra of all dispersions obtained at different sonication energy levels, it can be observed that the absorbance increases with sonication energy and reaches a plateau after a certain amount of supplied energy, which corresponds to the maximum achievable degree of CNT individualization in the aqueous solutions. This indicates that there is a minimum energy required to maximally disperse a given amount of CNTs in water, which is consistent with previous work reporting the effect of sonication conditions on the dispersion of CNTs in various solutions.[28,43] Noteworthy, the value of this minimum sonication energy is higher in the case of AL (i.e. ~150 kJ) than for SDS and CTAB (i.e. ~50 kJ), and yields a slightly higher maximum achievable degree of CNT individualization in water. Prolonged acoustic irradiation beyond this threshold is not only energy-consuming, but it also increases the likelihood of damaging the material. Higher sonication energy is known to induce damage and possibly cut the CNTs, which can have negative effects in several applications where CNTs with high aspect ratio are desired. The energy delivered to the solution is related to both sonication duration and amplitude, and it has recently been found that sonication time exhibits a much more pronounced effect on CNT shortening, while variations in the structural integrity of CNTs are

limited only to a minor extent with increased amplitude.[45] Prompted by this, a double acoustic irradiation system combining both bath and probe sonication is developed and investigated. Optical absorption spectra of the double-sonicated solutions (dashed lines) and the probe-sonicated specimens (straight lines) are compared in **Figure 2**. At low sonication energy (i.e. 25 kJ), a dramatic increase in absorbance is observed in the UV-vis region when the double sonication method is employed independently of the nature of the dispersant. The absorbance values obtained with double sonication at low energy match and even exceed those using traditional probe sonication at higher energy levels. This demonstrates that double acoustic irradiation improves the CNT dispersion process by drastically reducing the processing time while maintaining a very high degree of CNT individualization. The actual power used in the single and double sonication systems was estimated by measuring the temperature rise in an insulated bath in each case. Very little power imparted difference was observed between the use of the double-sonication system and the conventional probe sonication method. Therefore, resonance effects from the different sonication sources are suggested to induce synergies contributing to the enhanced dispersion of CNTs. At higher energy levels (i.e. 150 kJ), however, the effect of double sonication is contrasted and depends on the dispersant nature. In the case of SDS and CTAB, the utilization of double sonication at high energy levels yields quantities of single CNTs lower than and comparable to the maximum degree of CNT individualization achieved by typical probe sonication, respectively. For AL, the absorbance obtained by double acoustic irradiation at high energy is significantly increased in the whole UV-vis region with values exceeding the maximum achievable absorbance using traditional probe sonication. This is particularly interesting because this new maximum achievable degree of CNT individualization (i.e. estimated at 500 nm) for AL is more than 9 and 12% higher than that of CTAB and SDS, respectively. Such augmentation beyond the maximum

degree of CNT individualization achieved by typical probe sonication can be related to the propensity of lignin to associate into larger macromolecular complexes, which can provide greater repulsive forces between CNTs due to higher spatial volume and more steric hindrance. Acoustic irradiation is known to increase the degree of polymerization of lignin,[46] hence sonication-induced polymerization of lignin can enhance the dispersive efficiency of CNTs in water by increasing the spatial volume of lignin molecules adsorbed onto CNTs over the course of the double sonication process. A recent report also showed that higher molecular weight lignin leads to better CNT dispersion than lower molecular weight lignin fractions.[43] Therefore, the combination of AL with double acoustic irradiation provides an innovative way to both enhance dispersion quality and reduce processing time.

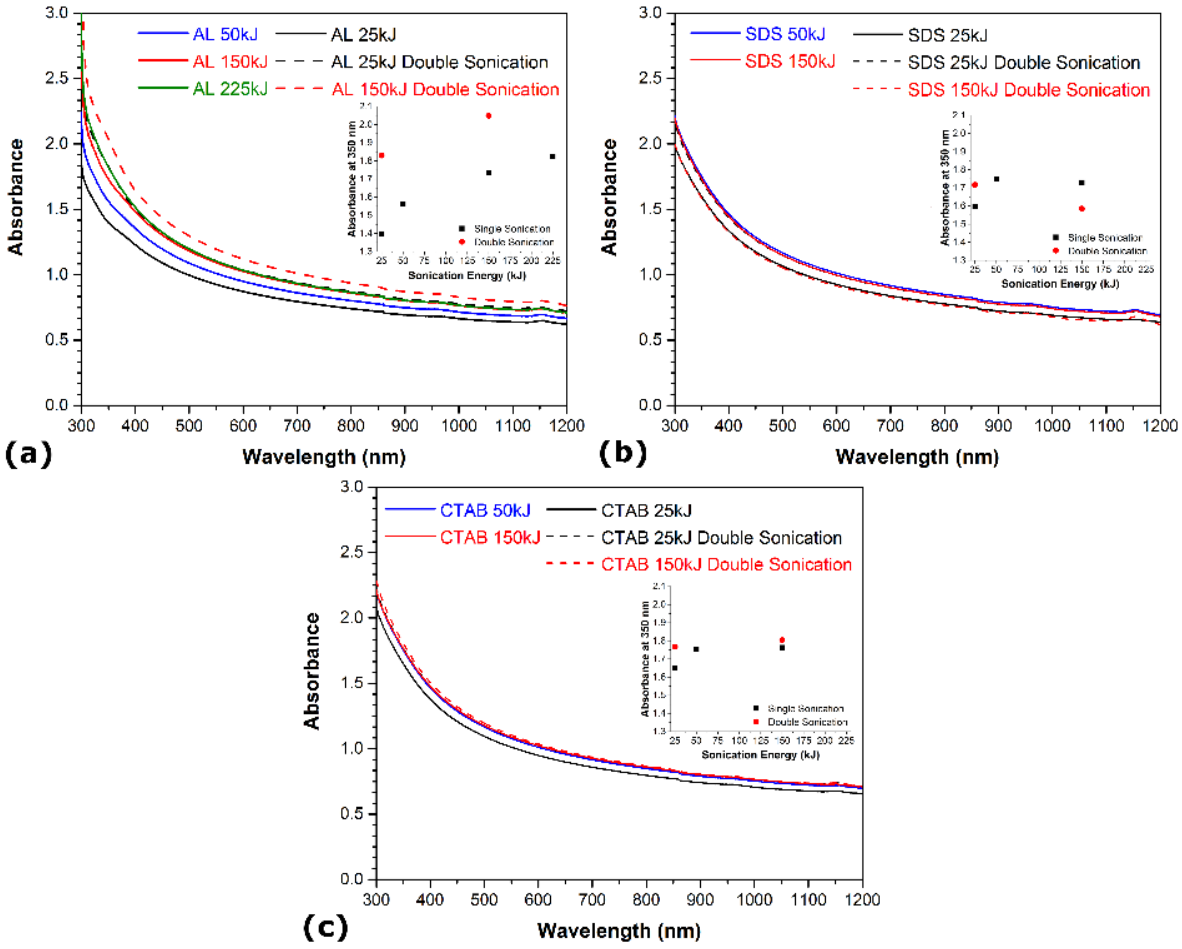

Figure 2. UV-vis spectra of different aqueous CNT dispersions as a function of the energy supplied to the solution: (a) AL, (b) SDS, and (c) CTAB. Straight lines correspond to probe sonication experiments, while dashed lines represents the double sonication system. Graphs of the absorbance at 350 nm as a function of sonication type and energy are shown in insets.

Influence of CNT functionalization and diameter

The influence of the CNT diameter and surface chemistry on the aqueous dispersion of CNTs are also examined. **Figure 3** shows the UV-vis spectra of the different suspensions prepared with the

materials listed in **Table 1**. In each case, the smaller CNTs (i.e. 8 nm in diameter) exhibit lower absorbance in the UV-vis region than the larger CNTs (i.e. 50 nm in diameter). In addition, the aggregates of undispersed 8 nm CNTs are larger than the aggregates of undispersed 50 nm CNTs (not shown). The surface contact between nanotubes being larger in the case of CNTs with smaller diameter due to higher surface area and aspect ratio, leads to stronger van der Waals attraction, hence hindering the dispersive efficiency.[47,48] Surface functionalization also shows a strong influence on the aqueous dispersion of CNTs. In the cases of no surfactant (**Figure 3a**), SDS (**Figure 3c**), and CTAB (**Figure 3d**), the presence of hydroxyl groups increases the absorbance in the UV-vis region. Noteworthy, the absorbance of the 8-nm functionalized CNTs is in the same range as that of the pristine CNTs with diameter of 50 nm. This indicates that surface-oxidized CNTs are easier to disperse than their non-functionalized counterparts under similar conditions. The presence of oxygen functional groups intercalated between the bundles generates stronger steric repulsion between CNTs and facilitates their debundling. This is consistent with recent molecular dynamics simulations showing that oxygen functional groups promote the confinement of polar solvent molecules between graphitic nanomaterials, resulting in higher solvent-induced repulsion for oxidized CNTs, which thus are less prone to aggregate.[49] Interestingly, the magnitude of the improvement depends on the CNT diameter – surface functionalization exhibits a much more pronounced effect on the dispersion quality of CNTs with larger diameter. In the case of AL suspensions, however, the influence of surface functionalization is contrasted. The presence of oxygen groups enhances the degree of individualization for the 50-nm CNTs, but it reduces dispersion quality for CNTs with smaller diameters (i.e. 8 nm). The increase in absorbance with surface functionalization for the larger CNTs is also sensibly lower than in the case of SDS and CTAB. These observations reveal that the diameter has a more prominent effect on the CNT

suspensions when AL is used as dispersant, while surface oxidation is more influential in SDS and CTAB solutions. This reflects the differences in how these molecules adsorb onto the surface of CNTs. The adsorption of SDS and CTAB surfactants on CNTs occur through electrostatic interactions, which is sensitive to surface oxidation. On the other hand, π–π interactions are responsible for the adsorption of AL on CNTs,[43] and larger diameter CNTs exhibit lower surface curvature which leads to stronger affinity to aromatic molecules due to higher overlap between π electrons.

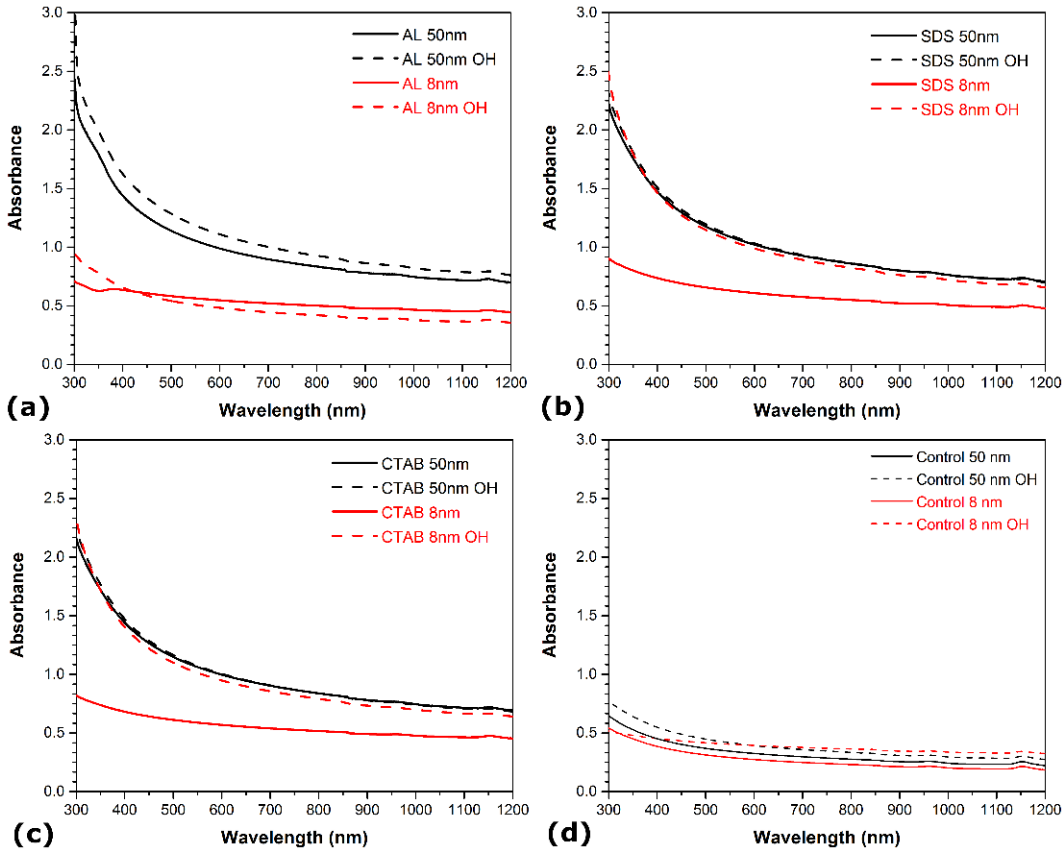

Figure 3. UV-vis spectra of different aqueous CNT dispersions as a function of CNT diameter and functionalization: (a) AL, (b) SDS, (c) CTAB, and (d) no surfactant.

Influence of dispersant mixtures

While most prior work about the aqueous suspension of CNTs have mainly focused on single surfactant solution, the use of mixtures of dispersants can be very effective. For instance, binary mixtures of SDS and CTAB have recently been found to induce synergistic effects improving surfactant packing on surfaces and modifications of repulsive/attractive forces.[37,50] Here, binary and ternary mixtures of different mixing ratios of AL/SDS, AL/CTAB, and AL/SDS/CTAB are studied. Based on the results described above (**Figure 1**), all solutions are prepared using a total surfactant to CNT mass ratio of 2:1. The optical absorption spectra of the binary and ternary mixtures are presented in **Figure 4a-b** and **Figure 4c**, respectively. In the case of both binary mixtures (i.e. AL/SDS and AL/CTAB), the AL:surfactant ratio of 90:10 achieves higher absorbance than the single dispersant solutions under similar conditions. Comparing the absorbance values of both 90:10 binary mixtures, it can be seen that the CNTs dispersed in the AL/SDS solution reach a higher degree of individualization. However, the use of surfactant mixtures does not necessarily guarantee an enhanced dispersing ability, as revealed by both binary mixtures at the AL:surfactant ratio of 80:20, which achieved the lowest absorbance among the different dispersant mixtures with values even below that of single surfactant solutions. Based on this observation, the ratio of AL is kept at a constant level of 90 in the ternary mixtures. **Figure 4c** shows the optical absorption spectra of the different ternary mixtures. While the 90:1:9 AL:SDS:CTAB mixture exhibits absorbance values below that of single surfactant solutions, the other ternary mixtures achieved the highest absorbance among all CNT dispersions under similar conditions.

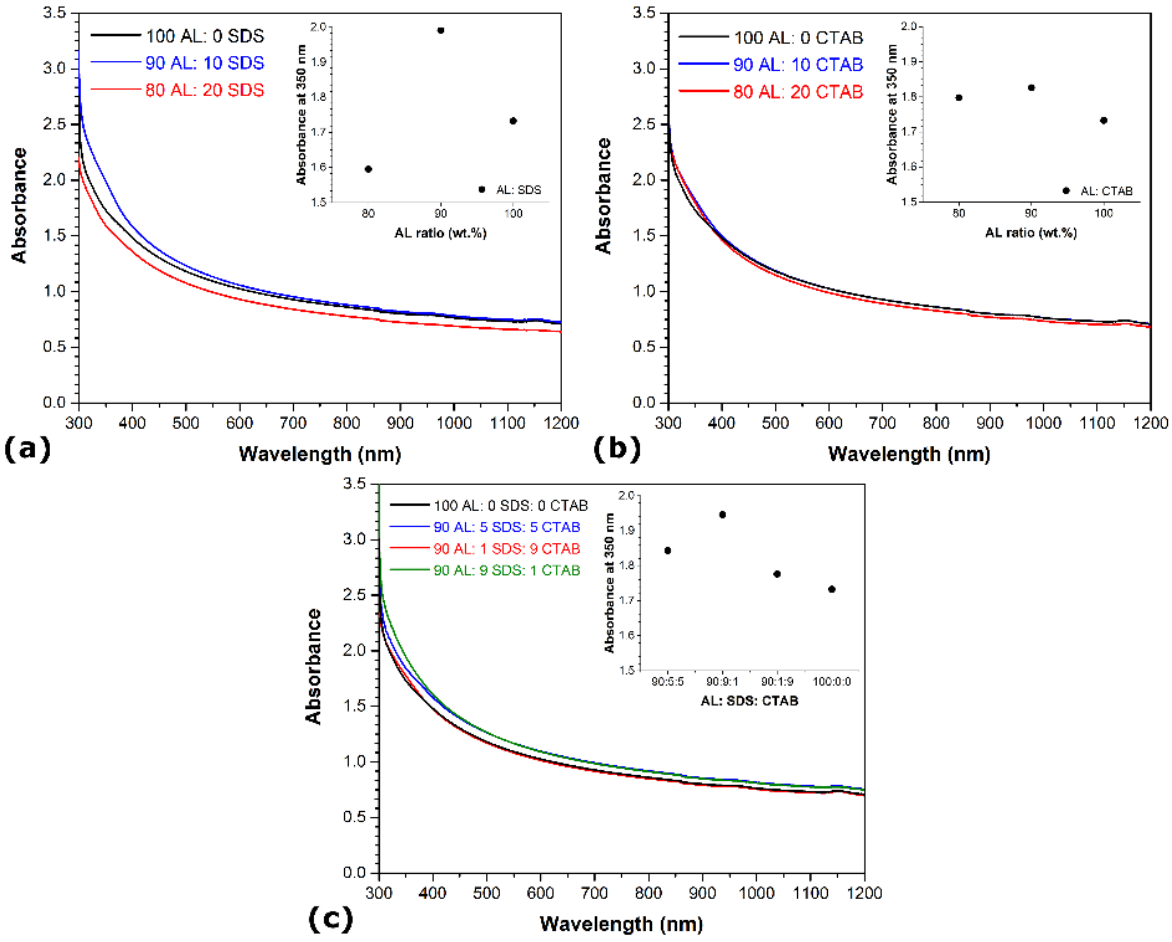

Figure 4. UV-vis spectra of aqueous CNT suspensions using different binary and ternary dispersant mixtures of (a) AL/SDS, (b) AL/CTAB, and (c) AL/SDS/CTAB. The absorption spectra of the CNT dispersion using pure AL (2 wt%) is added in each figure for comparison purposes. Graphs of the absorbance at 350 nm as a function of the surfactant composition are shown in insets.

The variations in absorbance due to the addition of CTAB and/or SDS to AL solutions suggests that interactions between these molecules largely contribute to the dispersing efficiency of CNTs in mixed dispersant solutions. The hydrophobic tails of SDS and CTAB molecules can bind to

hydrophobic surfaces of lignin, with the head groups that remain in the aqueous phase, providing stabilization by electrostatic repulsion.[51] This would limit the AL particle size and facilitate the access to adsorption sites located inside the small sonication-generated gaps between CNT bundles. The synergistic effects observed in the mixtures with CTAB can also arise from the electrostatic attractions between surfactants of opposite charge, which can improve dispersant packing onto the surface of CNTs.[37] However, higher concentrations of SDS or CTAB have been reported to induce the agglomeration of lignin into larger clusters,[51] which would result in the opposite effect on the adsorption of AL onto CNTs. Reduced surfactant adsorption onto the surface of CNTs ultimately translates to lower dispersion ability. It is also worth noting that the difference of absorbance between pure AL solutions and cationic-rich mixtures (i.e. CTAB ratio > 9) is lower than that between pure AL and anionic-rich mixtures (i.e. SDS ratio > 9). This can be attributed to the fact that AL and CTAB have opposite charges. Therefore, when both molecules adsorb onto CNTs, the charge neutralization leads to a reduction in the electrostatic repulsions between isolated CNTs.

Representative TEM images of different CNT suspensions depicted in **Figure 5** illustrate the role of AL in dispersing CNTs. The wet TEM specimens were prepared under the same conditions and various types of surfactants were utilized. In the absence of dispersant (**Figure 5**), CNTs are entangled and closely packed with one another, even after being exposed to 150kJ of sonication energy. When AL is introduced in the suspension under the same conditions, the degree of CNT individualization significantly increases, as shown in **Figure 5b**. Interestingly, it can be observed that some CNTs are partially separated and remain connected at one end, which further exemplifies the above described “unzippering” mechanism. In the case of dispersant mixtures (**Figure 5c**), all CNTs are completely individualized, hence demonstrating the superior dispersion efficiency of

surfactant mixtures. It is also worth noting that multiple CNTs have been damaged by high energy sonication, as demonstrated by the magnified view in the inset and by the large number of short CNTs (<5 μm).

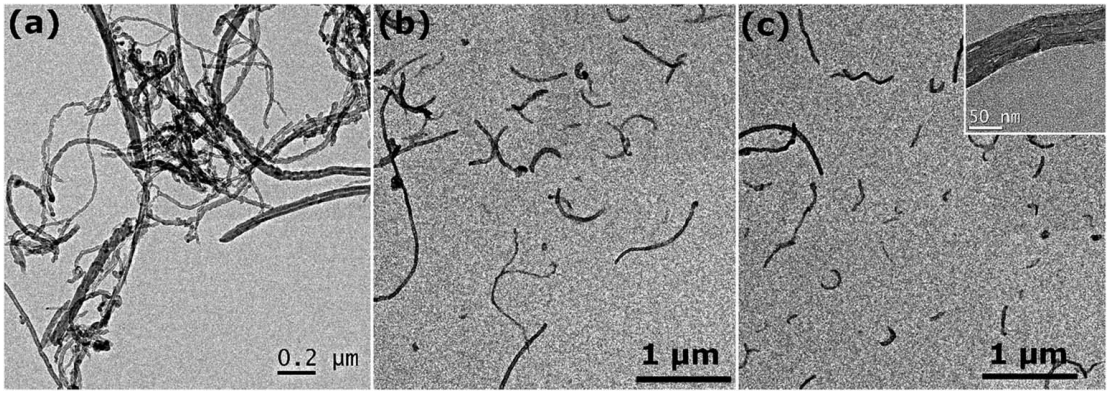

Figure 5. Representative TEM images of aqueous dispersions of 50 nm diameter CNTs (a) without any surfactant, (b) with AL, and (c) with a ternary mixture of AL/SDS/CTAB (90 : 9 :1).

Colloidal stability of different CNT dispersions in water

The settling velocity of the aqueous CNT dispersions with pure, binary and ternary surfactants is investigated. While pure CNT suspensions without any dispersant settle down after only few hours, no sedimentation is observed by visual examination of the solutions by the naked eye when surfactants are employed. The dispersion state of the different suspensions as a function of time is characterized by both UV-vis spectroscopy and optical microscopy over a 34-day period, and results shown in **Figure 6** serve as indicators of colloidal stability. Although the absorbance at 500 nm of all specimens drops in this time period, the most dramatic decreases are observed in the pure SDS and CTAB dispersions with variations up to 21%, which is more than twice the variations of the AL-containing samples (i.e. <10%). Moreover, except for the ternary dispersant mixture where

the absorbance gradually decreased over time, all other AL-containing specimens exhibit relatively stable absorbance values in the 34-day time period. These results are consistent with light microscope analysis, as depicted in **Figure 6a,b,d**. The aggregates observed in the dispersant mixtures (i.e. both binary and ternary solutions) are all smaller than 40 μm, while an increasing number of aggregates larger than 50 μm is found over time in the pure surfactant solutions. The slower settling process of AL-containing suspensions can be attributed to the higher degree of CNT individualization in the solutions, but also the higher viscosity of AL compared to SDS and CTAB. To further study colloidal stability of AL-CNT solutions, the suspensions are dried in air at 50°C and re-dispersed in DI water in concentrations ranging from 0.5 wt % to 2 wt%. The dried CNT powder spontaneously re-disperse itself in water without the need for stirring or sonicating. The resulting suspensions remain stable over several weeks, and centrifugation at 5000 rpm for 30 min does not induce the precipitation of CNTs. The spontaneous re-dispersion of the dried CNTs in water and their stability at high concentrations are indicative of steric stabilization. Hence, these results demonstrate that the use of AL, either alone or in mixtures with other dispersants, not only achieve a higher degree of CNT individualization in water, but also exhibit enhanced colloidal stability for several weeks compared to traditional petrochemical surfactants.

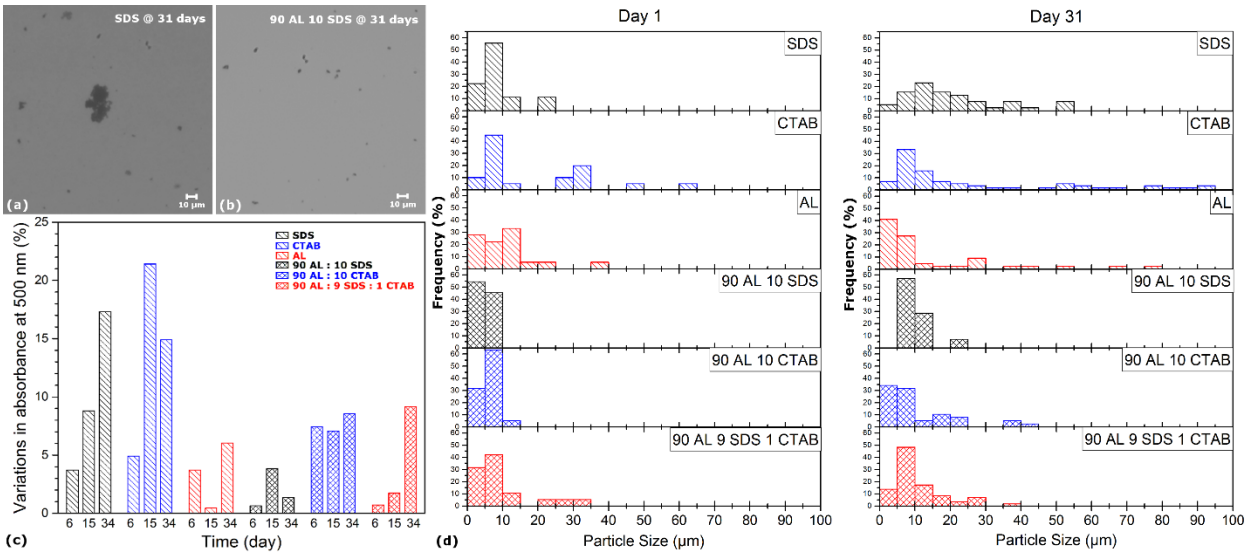

Figure 6. Representative optical micrographs of aqueous CNT dispersions using (a) SDS and (b) AL/SDS after 1-month sedimentation. (c) Colloidal stability of CNTs suspended in water using different pure, binary, and ternary mixtures of dispersants. (d) Particle size distributions of the different aqueous CNT dispersions after 1-day and 1-month sedimentation.

After processing, the removal of dispersant is usually required in various applications as most surfactants, such as SDS or CTAB, can have detrimental effects on multiple characteristics of the final material. The addition of lignin, however, is known to improve the thermo-mechanical properties of various types of cements, concretes, and polymer composites.[52] Lignin can act as an adhesion promoter for the formation of highly enhanced interfaces between individualized CNTs and a polymeric matrix. Should the removal of AL be desired for a specific application, it can be efficiently achieved by a simple thermal treatment, as demonstrated in **Figure 7**. When the dried AL-CNT powder is annealed in air at 300°C for one hour, it does not spontaneously re-dispersed in DI water and settles down almost instantly after stirring. The Tyndall effect is no longer visible

in the re-dispersed suspension after annealing, which means that colloidal particles are not present in the solution, indicating that AL has been fully removed during thermal treatment.

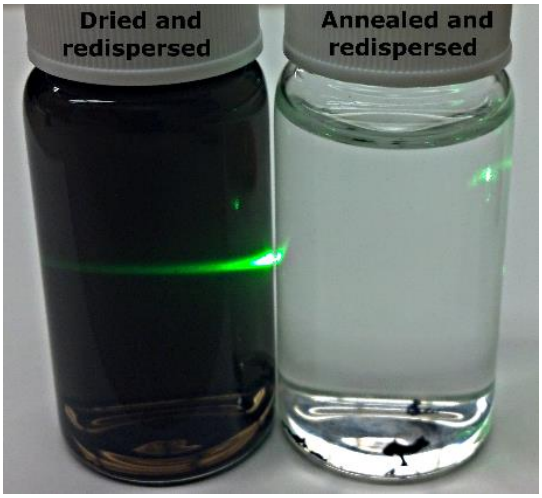

Figure 7. Vials containing re-dispersed CNTs in water after drying (*left*) and after annealing at 300 °C in air for one hour (*right*). Note that in the right image CNTs coagulate at the bottom and the Tyndall effect is not visible, demonstrating the absence of colloidal particles in water.

CHAPTER 2: Graphene impregnated wood filters for sustainable water purification

Increased populations and industrialization has led to an increase in the release of contaminants, such as organic dyes, into natural aquatic systems. This increased release of contaminants is a leading cause in a variety of environmental hazards and water pollution. While the hazards and health effects associated with these dyes include toxicity, carcinogenic effects and long term stability, organic dyes such as methylene blue (MB) are still widely used in a variety of industries,

including textiles, pulp and paper, and biomedical fields.[53,54] It is of paramount importance to efficiently remove dyes from aqueous solution using an effective and inexpensive technique. Continuous flow adsorption of MB by nanosorbent impregnated wood templates was examined due to its low cost and opportunity for practical application into industrial waste treatment processes.

The mesoporous structure of wood is inherently designed to facilitate bulk water treatment due to the existing network of partially aligned, hollow vessels that are interconnected through a series of pores. This existing network enables the continuous flow of water, ideal for a continuous adsorption process. Basswood templates were selected for their high porosity (50% pore volume)[55] and impregnated with an aqueous solution of GnPs and AL as AL was previously proven to have effective dispersing capabilities on graphitic structures. By immobilizing the AL coated graphene nanoplatelets (GnPs) within the woods three-dimensional structure, the high surface area of GnPs was preserved by further minimizing agglomeration effects, allowing for increased contact time with methylene blue (MB) throughout the entirety of the continuous adsorption study.

Experimental method

Materials and chemicals

Tilia americana (basswood) was purchased from Crosscut Hardwoods. Graphene nanoplatelets (GnPs) were obtained from Sigma Aldrich with surface area 750 m^2/g as per the manufacturer technical data. The alkali lignin (AL, 99%) and methylene blue (MB, 99%) were purchased from Tokyo Chemical Industry Company and TCI America respectively. HPLC grade acetone was purchased from Fischer chemical with a purity greater than 99.5%. All dispersions were conducted using deionized (DI) water and all materials were used as received without any further treatment unless otherwise specified.

Preparation of GnP-decorated basswood filters

Aqueous dispersions of GnPs pre-adsorbed with AL were prepared by double acoustic irradiation following a previously established procedure.[30] Briefly, 0.5g of AL was first dissolved in 200 mL DI water using bath sonication for 15 minutes at 25 °C. Then, pristine GnPs were added to the AL solution, at a ratio of GnP:AL 2:1 w/w and the mixture was sonicated using a double acoustic irradiation system for 45 minutes. The as-prepared GnP dispersions were loaded in basswood discs of 29 mm diameter and 6 mm thickness using a vacuum impregnation method. Prior to GnP impregnation, the wood discs were sonicated in acetone for 30 minutes and rinsed with DI water to remove extractives and other organic impurities. The washed wood discs were oven dried at 60 °C for 2 hours and sealed in a vacuum chamber. The aqueous GnP suspension was introduced under vacuum, dropwise onto the wood surface, allowing for capillary action to pull the GnP solution into the wood porous structure. After drop casting 200 mL GnP dispersion, the wood disk remained under vacuum in solution for 24 hours. After GnP impregnation, each wood filter was cut in half such that the thickness was reduced to 3 mm, and thoroughly washed using alternating DI water and acetone to remove any un-adsorbed GnPs. Washing was monitored by UV-Vis absorption spectroscopy and was conducted until no appreciable change in the filtrate was observed with additional rinsing.

Characterization of microstructure and physical properties

The morphology of as prepared wood filters was examined by optical and electron microscopies using a Zeiss Axiocam ERc5s digital camera mounted on a Zeiss Axiolab light microscope and a Sirion XL30 electron microscope. For scanning electron microscopy, the samples were coated with a gold-palladium layer and the observations were conducted under high vacuum conditions at an accelerating voltage of 5 kV. To probe the distribution of GnPs in the wood filters, Raman spectra

were recorded at various positions over the range of 900-1800 cm^{-1} with a spectral resolution of 1 cm^{-1} by a Renishaw InVia Raman microscope equipped with a 785 nm laser. UV-vis absorption spectroscopy measurements were performed in quartz cuvettes using a Perkin Elmer Lambda 750 spectrophotometer operating in the 200-1200 nm range with a spectral resolution of 1 nm.

Adsorption studies

Continuous flow studies

Wood filters were wrapped with Teflon tape and fitted into 29-mm diameter rubber caps, which were sealed into the bottom of a 140 cc monojet syringe. The syringe system was equipped with a 74900 Cole Palmer liquid flow controller and placed in a vertical position, as illustrated in **Figure 8**. The filters were first wet with 100 mL of DI water, before aqueous solutions of methylene blue were pumped through the wood. Three feed concentrations of methylene blue, C_0, (i.e. 10, 12, and 14 mg/mL) and three liquid flow rates (3.0, 3.5, and 4.0 mL/min) were examined and adsorption data were systematically analyzed in a 3^2 factorial design where all combinations of MB concentrations and flow rates were tested with triplicate centroid conditions, as listed in **Table 2**. The filtrate concentration at the outlet of the syringe, C_t, was measured at different time intervals by UV/vis absorption spectroscopy using a measured extinction coefficient from Beer's law analysis at the maximum absorption peak for MB (i.e. 664 nm). Filtrate samples were collected every minute until breakthrough was reached, and every five minutes henceforth. Breakthrough is expressed in terms of normalized concentration (i.e. C_t/C_0) and was declared when the ratio of the filtrate concentration over the feed concentration reached 0.1. This value was selected to reflect the regulation limit for MB levels in humans and aquatic species established by the National Institutes of Health and the National Center for Biotechnology Information (i.e 2mg/kg). All experiments were conducted at 25 °C for the time required to treat 100 mL of MB solution at each

designated flow rate. After treatment of 100 mL MB solution, the cumulative filtrate concentration was measured by UV-vis absorption spectroscopy. Long-term experiments were also performed by refilling the syringes with another 100 mL of the same feed solution multiple times until complete saturation of the wood filters was achieved. The Thomas and Yan models were fitted to the experimental, long-term adsorption data using Origin 8.0 software[56,57]. For comparison purposes, experiments were conducted under the same conditions using wood discs in the absence of GnPs. Similarly, 140 cc monojet syringes were also packed with 0.5 g GnP powder to the same depth as the wood filters (i.e. 3 mm). The GnPs were supported and surrounded by polyester fibers to prevent bed expansion during treatment.

Table 2. Centroid design with center point replicated two times

	MB Concentration (mg/L)	**Flow Rate (mL/min)**
1	10	3.0
2	12	3.0
3	14	3.0
4	10	3.5
5*	12	3.5
6*	12	3.5
7*	12	3.5
8	14	3.5
9	10	4.0
10	12	4.0
11	14	4.0

*denotes a triplicate of the centroid point

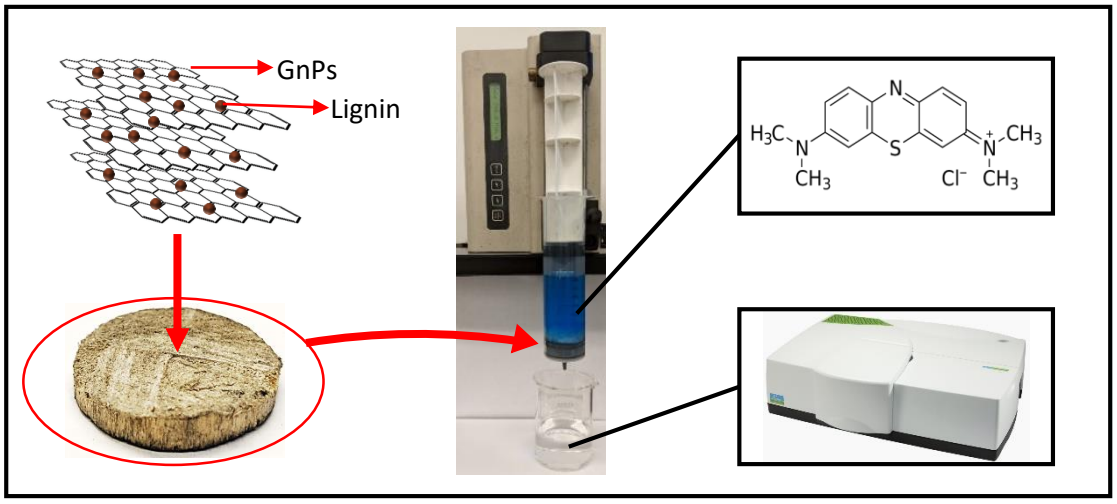

Figure 8. Experimental setup for the continuous adsorption of MB from synthetic contaminated water by GnP wood filters.

Batch treatment

Aqueous solutions of MB were prepared at concentrations of 10, 12, and 14 mg/mL with a pH of 8.02 monitored with an EcoSense pH10A pH-meter. Dried powders of GnPs with a mass of 0.5 g were added to 100 mL MB solution. The mixtures were placed on an orbital shaker operated at 120 rpm for 20 minutes. The contact period (i.e. 20 minutes) was chosen based on the time required to treat 100 mL of solution at a given flow rate (i.e. 4.0 mL/min) in the continuous flow system. After 20 minutes, the supernatant was decanted away and the MB concentration was measured by UV-vis absorption spectroscopy. The amount of MB adsorbed per mass of GnP, q (mg of MB per g of GnP), was determined by subtracting the mass of MB in solution after 20 minutes from the initial mass of MB in solution.

Regeneration of wood filters

After completing the treatment of the first 100mL MB solution at 4.0 mL/min, the wood filters were removed from the syringe and washed with copious amounts of acetone until no appreciable

change was observed by UV-vis absorption spectroscopy. The regenerated wood filters were then re-sealed back into the bottom of the syringe and tested for another 100 mL of MB solution under the same operating conditions (i.e. 14 mg/mL, 4.0 mL/min). A total of five successive adsorption/desorption cycles was conducted and the cumulative filtrate concentration was measured by UV-vis absorption spectroscopy at the end of each treatment cycle. The effectiveness of the solvent regeneration was assessed based on the regeneration efficiency (RE) and the step stripping efficiency (SSE) defined as

$$RE\ (\%) = \frac{q_i}{q_0} * 100 \quad (1)$$

$$SSE\ (\%) = \frac{q_i}{q_{i-1}} * 100 \quad (2)$$

where q_i (*mg/g*) indicates the adsorption capacity of any given cycle *i*, q_{i-1} (*mg/g*) indicates the adsorption capacity the cycle preceding the current cycle, and q_0 (*mg/g*) indicates the adsorption capacity of the initial cycle prior to any solvent regeneration.[58]

Results and discussion

Wood filter characterization

The structure of the wood filters before and after GnP impregnation was examined by scanning electron microscopy, as illustrated in **Figure 9**. Hardwoods, such as the basswood used in this study, are comprised of a complex mesoporous structure of long, partially aligned channels in the length direction referred to as vessels. The vessels can have diameters up to several hundred micrometers and are uniquely designed to transport fluid throughout the wood.[55] Laterally aligned vessels are connected through pits, or holes in the side walls that allow for water transport perpendicular to the vessel direction, allowing for fluid to be transported in all directions throughout the wood structure. As vessels can comprise up to 60% of the wood by volume, water

treatment is a reasonable application for hardwoods such as the basswood used in this study as the vessels enable continuous fluid transportation.[55] The structure of pristine basswood samples can be seen in representative digital and SEM images in **Figure 9a-c**. In the impregnated specimens shown by the representative optical and SEM images in **Figure 9d-f**, the GnPs have been deposited onto the walls of the vessels and pits and immobilized on the basswood template. The GnPs achieved a reasonable distribution along the vessels with minimal agglomeration, and no blocking of the vessel diameter. This allows for contaminated water to adequately flow through the vessels and pits, contacting the immobilized GnPs, promoting adsorption.

A reasonable mechanism for the depositing of GnPs on the vessel walls is that the aromatic rings on the GnP are able to adsorb onto the aromatic rings in the cellulose within the wood structure through $\pi - \pi$ stacking.[59,60]

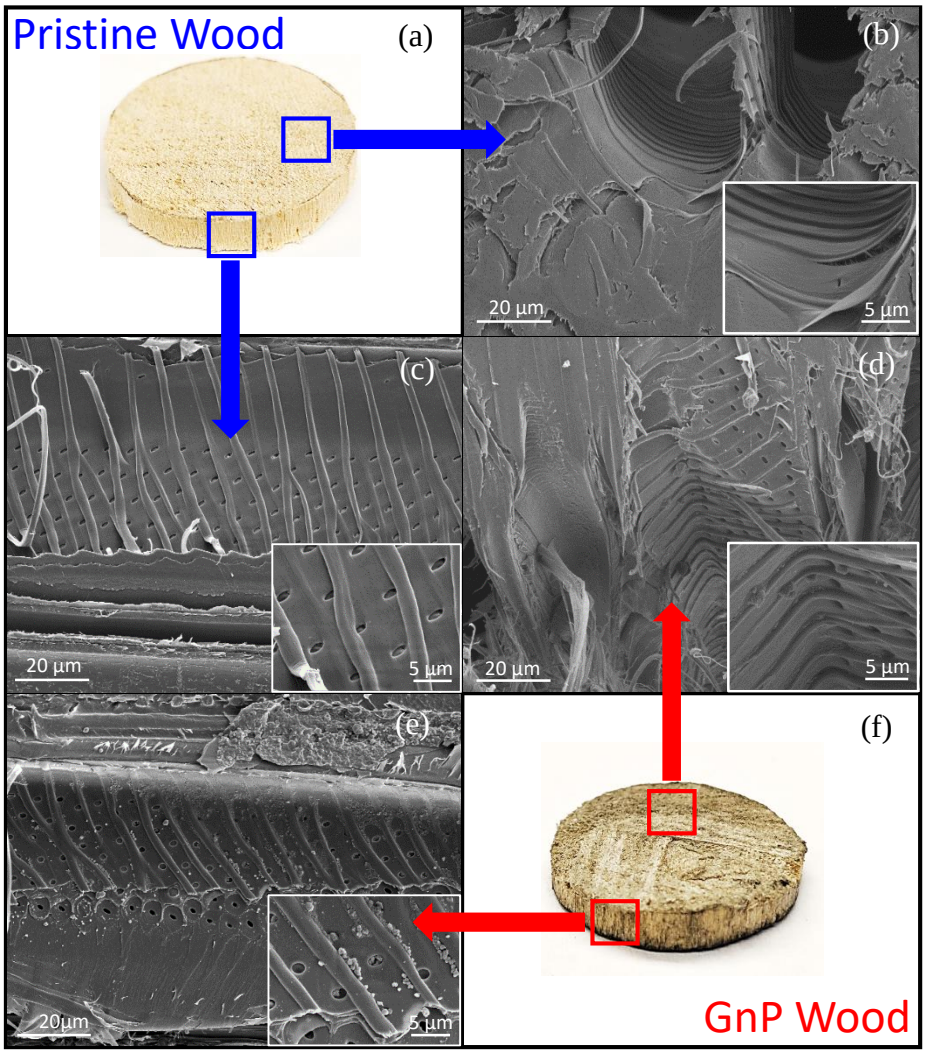

Figure 9. Representative photographs and SEM micrographs of 3-mm thick pristine (a-c) and GnP-impregnated (d-f) basswood discs, with transverse (b,d), and longitudinal (c,e) views.

The distribution of GnP within the wood vessels can be attributed to the vacuum impregnation method used to disperse the aqueous GnP solution throughout the wood filters by pulling the GnPs into the wood and through the full length of the vessels. While GnPs were able to penetrate the full thickness of the wood filters, there was still a distribution gradient of GnPs from the outside

edge of each filter to the center. Optical microscopy images quantified using ImageJ software depicted in **Figure10**, were used to determine the average number of GnPs found through the full thickness of the wood filters when divided into 5 sections of equal area. The GnP loading decreased when progressing through the thickness of the wood filter from position 1 (P1) to position 5 (P5) shown by the bar graph in **Figure 10a**. Raman spectroscopy results shown in the insets for positions 1, 3, and 5, also confirmed the presence of a higher quantity of GnP at the top of the wood filter (outside) than at the bottom (inside,) shown by the higher intensity characteristic D and G graphene peaks at 1350 and 1580 cm^{-1} respectively.[61] The D peak intensity ratio between position 1 and position 5 was 13.8, indicating there was more than ten times the amount of GnP present at the top of wood filters than at the bottom.

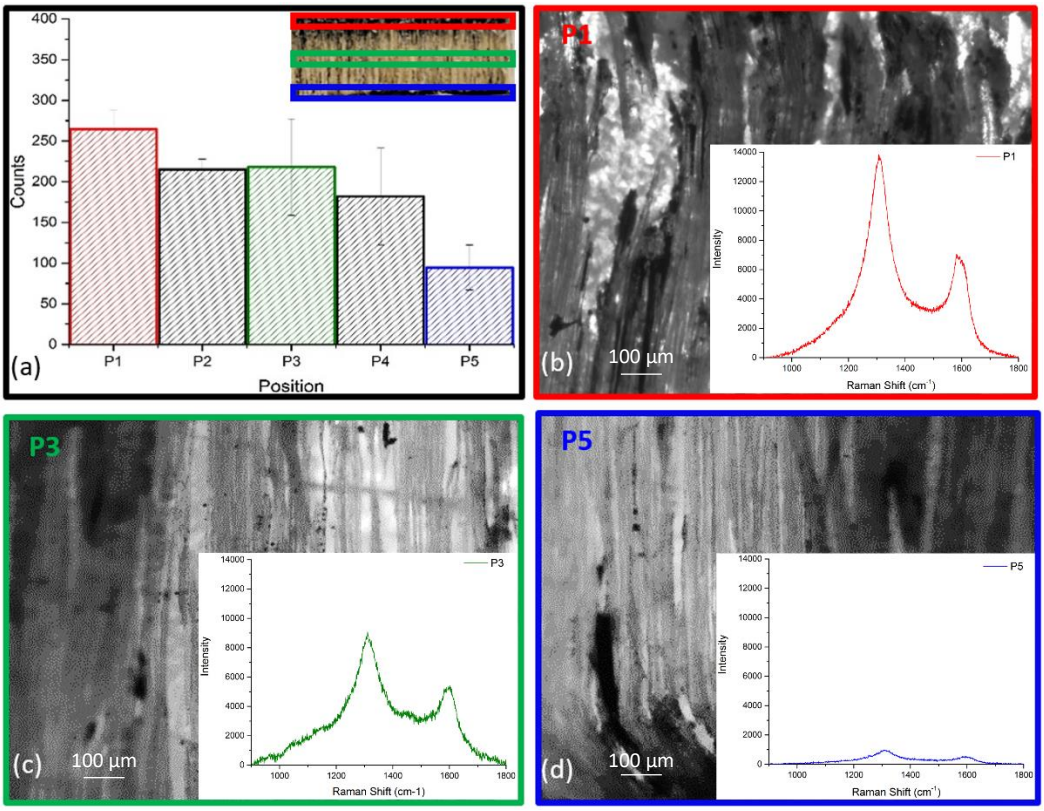

Figure 10. (a) ImageJ software analysis of GnP particle counts across 5 different sequential positions in the through thickness direction of filter. Representative optical microscopy images and Raman spectra (insets) depicting GnP distribution gradient across (b) position 1, (c) position 3, and (d) position 5.

Effect of MB concentration and flow rate on cumulative filtrate concentration

The color change from blue to clear observed during all continuous adsorption studies is attributed to the adsorption of MB from the feed solution onto the GnPs embedded in the vessels of the wood. Prior to testing GnP wood discs, pristine wood discs were first tested to determine the effect, if any, that the cellulose fibers in the wood itself had on the adsorption of MB from aqueous solution. Representative UV-vis spectra of the cumulative filtrate concentration after 100 mL of MB

contaminated water had been pumped through pristine and GnP wood discs are shown in **Figure 11**. Compared to the concentration of the feed solution, the effluent concentration of the pristine wood showed minimal change as represented by the UV-vis spectra and the visual lack of color change in solution show by the inset in **Figure 11a**. There was however a distinct color change and reduction in the characteristic MB peak from the feed to the effluent of the contaminated water treated with the GnP wood disc, shown in **Figure 11b**. This suggests that the GnP is the active material promoting the adsorption of MB from aqueous solution, rather than the wood itself. The adsorption of MB by the GnPs can be reasonably attributed to π-π stacking due to the aromatic rings in both the MB and the GnPs.[59,60]

Batch and fixed bed adsorption studies using GnP powder were also conducted to determine the effect that the wood template had on the adsorption capacity of the GnPs. The effectiveness of each type of adsorbent, GnP wood, pristine wood, and GnP powder in batch and fixed bed systems was determined by the removal efficiency (RE) and cumulative normalized filtrate concentration ($\frac{C_{t=20}}{C_0}$), after treatment 100 mL of MB solution. All comparative adsorption studies were tested at a 10 mg/L feed MB concentration and a flow rate of 4.0 mL/min for wood and fixed bed studies. In the pristine wood study the adsorbent mass was taken as the mass of the wood filter. In the GnP wood study the adsorbent mass was taken as the mass of GnPs in the wood filter, which was estimated as 0.07g based on the total mass of GnPs present during the vacuum impregnation minus the GnPs removed during washing. The adsorbent mass for the fixed bed and batch study was taken as the 0.5g of GnP powder used. This mass of GnP powder was selected as it equates to filling the same volume in the column as the Gnp impregnated wood filters used during the continuous adsorption experiments, resulting in approximately the same bed depth of 3 mm for both the continuous flow and fixed bed adsorption studies. Prior to all fixed bed and continuous

adsorption studies, one full syringe (100 mL) of DI water was pumped through the filters and showed that after the full volume no GnP was detected in the effluent. Results from the comparative adsorption study are shown in **Figure 11c**.

As expected, the pristine wood filter had the lowest removal efficiency and therefore the highest cumulative normalized MB concentration in the filtrate among all materials tested, reaffirming that the GnP is the active adsorbent in the system. The fixed bed study (packed GnP powder) resulted in a slightly higher removal efficiency (87.4%) than its batch counterpart (72.5%). This is consistent with literature reports as the difference between batch and continuous flow processes can be explained by the fact that, in a dynamic system, the adsorbent is in equilibrium with the feed concentration, while in a batch process, the adsorbent is in equilibrium with the residual concentration, which is necessarily less than the feed concentration. Such variations in concentration can lead to significant changes in uptake values, as concentration gradient is a driving force for adsorption.[62] As the same amount of adsorbent was used in both the batch and fixed bed study, it is reasonable that the fixed bed study resulted in a higher removal efficiency than the batch process. Both the batch and fixed bed processes also resulted in a cumulative normalized filtrate concentration greater than breakthrough (0.1), indicating that more adsorbents are needed to meet environmental and toxic limit regulations. The GnP-impregnated wood filter however, maintained a cumulative normalized filtrate concentration below 0.1, and resulted in the highest removal efficiency of 91.1%, despite having the least amount of active adsorbent (GnP) present. This enhanced performance is most likely attributed to the ability of the wood template to immobilize the GnPs and preserve their high available surface area by minimizing aggregation.

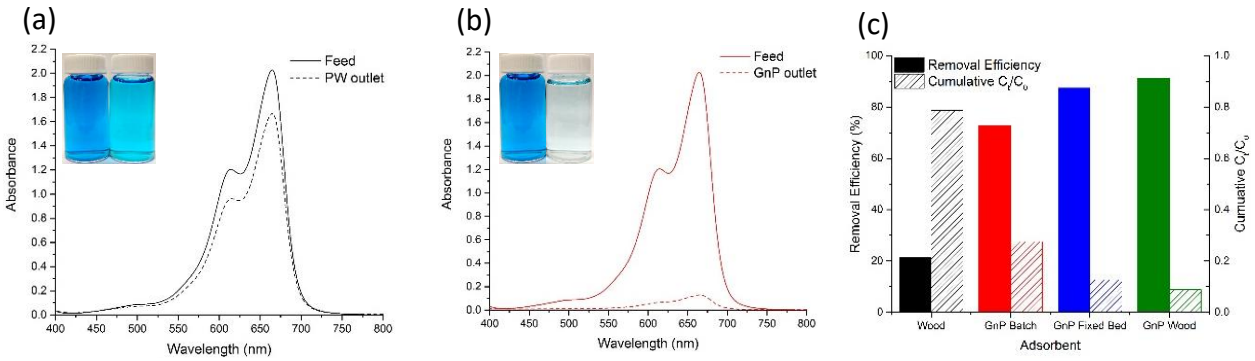

Figure 11. (a) Representative UV-vis spectra of feed and effluent absorbance of water treated by pristine wood disk. Inset shows visual representation of color change from feed to effluent solution and (b) Representative UV-vis spectra of feed and effluent absorbance of water treated by GnP wood disc. Inset shows visual representation of color change from feed to effluent solution. (c) Representative adsorption capacity (q) and normalized cumulative filtrate concentration (C_t/C_0) for batch, fixed bed, and continuous adsorption studies.

Modeling of continuous adsorption study

The effectiveness at GnP wood filters on MB adsorption in a continuous system can be evaluated from the breakthrough curve of the normalized filtrate concentration. The breakthrough curves explain the loading ability of an adsorbent.[63] Breakthrough curves plot the normalized filtrate concentration (C_t/C_0) as a function of the volume or in the context of this study, the time in which an adsorbent has been used for. Two simplified nonlinear models, including the Thomas and Yan models, were employed to analyze the experimental results from the continuous adsorption study. The Thomas model is one of the most widely used kinetic theory models for column adsorption, written as follows[56]

$$C_t/C_0 = \frac{1}{1 + e^{(\frac{k_{TH} q_0 M}{Q} - k_{TH} C_0 t)}} \quad (3)$$

where $C_o\ (mg/L)$ refers to the inlet MB concentration, $C_t\ (mg/L)$ refers to the filtrate MB concentration at any time *t (min), Q* (*mL/min*) is the inlet flow rate, *M* is the mass of adsorbent in *(g),* and $k_{TH}\ (mL/min * mg)$ and $q_0\ (mg/g)$ are the Thomas rate constant and maximum adsorption capacity, respectively. GnP filters adsorption data was fitted to the Thomas model using Origin 8.0 software. The resulting parameters from this study for a GnP filter tested at 14 mg/L and 4.0 mL/min until saturation was reached are shown in **Table 3**.

The Yan Model, in nonlinear form can be expressed as[57]

$$C_t/C_0 = 1 - \frac{1}{1 + (\frac{Q^2 t}{k q_0 M})^{(kC_0/Q)}} \quad (4)$$

where $C_o\ (mg/L)$ refers to the inlet MB concentration, $C_t\ (mg/L)$ refers to the filtrate MB concentration at any time *t (min), Q* (*mL/min*) is the inlet flow rate, *M* is the mass of adsorbent in *(g),* and *k* (*L/mg*min*) and q_0 (*mg/g*) refer to the Yan model constant and maximum adsorption capacity respectively. The fitting results from the Yan model breakthrough curve of a GnP filter tested at the highest inlet MB concentration and flow rate (14 mg/L and 4.0 mL/min) until saturation was reached are shown in **Table 3**. All Yan models were fitted to the experimental continuous column adsorption study data using Origin 8.0 software.

Table 3. Results from nonlinear kinetic column models for GnP wood filter used in continuous column adsorption study tested at 14 mg/L and 4.0 mL/min.

	M (g)	**C_0 (mg/L)**	**Q (mL/min)**	**k (V/min*mg)**	**q_0 (mg/g)**	**R^2**
Thomas	1.3395	14	4	1.46427 (mL)	2.9695	0.79355
Yan	1.3395	14	4	242.73402 (L)	2.37748	0.99001

As seen from the breakthrough curve results in **Figure 12**, the Yan model was found to fit the experimental adsorption data better than the Thomas model, with an R^2 value of 0.99. The Yan model most likely fit the data better as it is able to overcome a main drawback of the Thomas model in its deficiency to estimate the normalized filtrate concentration at time zero.[64] The Yan model was therefore used to accurately predict the time at which GnP filters tested within the centroid design framework, would reach breakthrough. As breakthrough is typically set close to 0, or at a threshold some percentage below an environmental or medical limit for exposure, it is indicative of when an adsorbent would need to be regenerated or replaced.[65] In the context of this study, breakthrough was set at 0.1 (1.4 mg/L) as the NCBI suggests 2mg/kg as the threshold for toxicity levels in humans.[66] This would allow for approximately one liter of contaminated solution to remain below the recommended toxicity levels if ingested, per kilogram of body mass. Saturation was set at 0.75, representative of when the filter has become completely spent, allowing for the majority of MB in the influent to be passed through the filter un-adsorbed and released into the effluent.

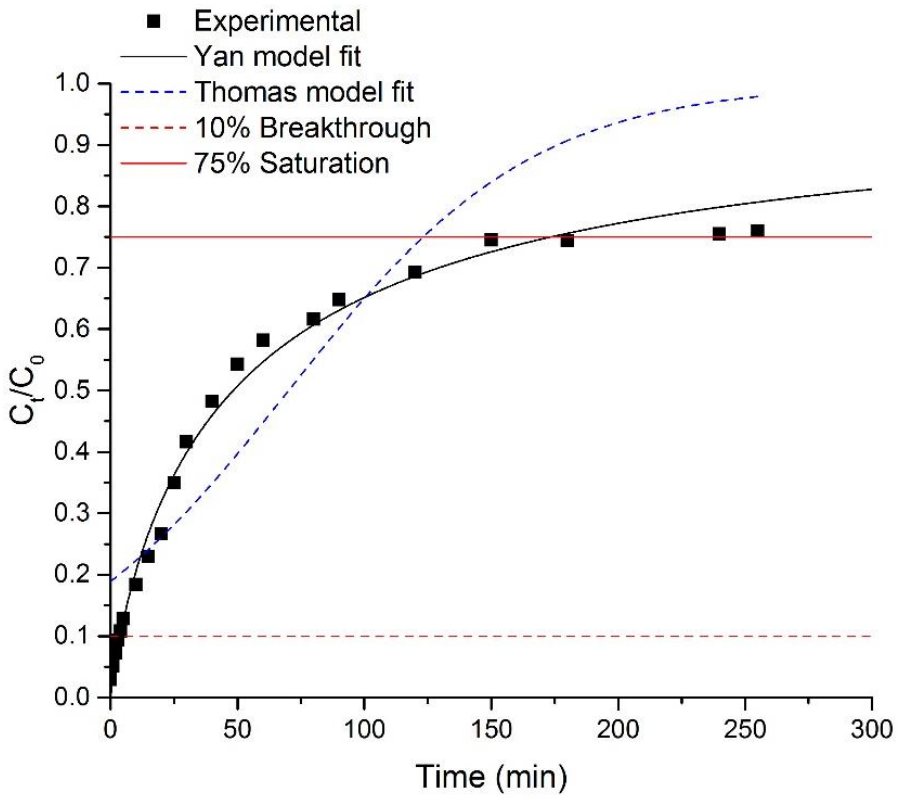

Figure 12. Breakthrough curve for GnP filter tested at 14 mg/L and 4.0 mL/min inlet parameters. Solid black line represents Yan model fit and dotted blue line represents Thomas model fit. Horizontal dotted and solid red lines indicate breakthrough (0.1) and saturation (0.75) respectively.

The Yan model was also used to estimate the maximum adsorption capacity of the GnP-impregnated wood filter, when the filter had reached exhaustion. This value was found to be 45.5 mg/g, which is comparable, if not higher than most previously reported adsorption capacities for MB in the literature for various adsorbents in continuous flow processes, as listed in **Table 4**.

Table 4. Comparison of the adsorption capacity in fixed bed systems for the removal of MB from aqueous solution on different adsorbents.

Adsorbent	C0 (mg/L)	Q (mL/min)	q (mg/g)	bed depth (cm)	Reference
GnP wood (continuous)	10	4	45.45	0.3	this study
GnP	10	4	1.70	0.3	this study
rice husk	50	8.2	4.41	25.4	[67]
natural zeolite	30	2.2	4.30	15	[68]
graphite oxide coated sand	100	2	0.95	15	[69]
CNC-alginate hydrogel beads	200	4.17	255.50	7.4	[70]
silica sands	50	2.683	5.35	-	[71]
microwave assisted CNTs	2	-	45.66	2	[72]
valorized olive stones as AC	100	3	107.40	3	[73]

While some reported adsorbents achieved higher adsorption capacitates than were determined in this study, the majority of adsorbents used required significant pretreatment to effectively modify the adsorbent surface for MB adsorption. In this study as-received GnPs were combined with AL in aqueous solution and then directly impregnated in basswood templates. The GnP impregnated wood filters were able to achieve a relatively high adsorption capacity with minimal pretreatment and chemical modification, while capitalizing on the naturally existing mesoporous structure of the wood, inherently designed to facilitate bulk water treatment.

Effect of inlet MB concentration and flow rate on breakthrough and cumulative normalized filtrate concentration

Linear and quadratic models were fit to the time taken to reach breakthrough as a function of the inlet MB concentration and flow rate for each GnP wood filter. The quadratic model

$$Breakthrough = -0.333(\pm 0.559)x^2 + 4.517(\pm 13.436)x + 6.945(\pm 8.944)y^2 - 60.876(\pm 62.676)y + 133.126(\pm 116.719) \quad (5)$$

was found to fit the data more accurately than the linear model with an R^2 value of 0.87. The analysis of variance table for this analysis is shown in **Table 5**. Even though a large amount of standard error was observed for the majority of GnP filters, the calculated F value was larger than the critical F value, indicating that this regression is statistically significant at a 95% confidence level. The surface response for this model is given in **Figure 13a** and shows that the highest breakthrough time was observed for GnP filters tested at the lowest inlet MB concentration and flow rate.

Table 5. Analysis of variance table for breakthrough time as a function of inlet MB concentration and flow rate.

	df	**SS**	**MS**	**F Value**	**Prob>F**
Regression	5	2009.219	401.844	31.726	3.56E-04
Residual	6	75.997	12.666		
Uncorrected Total	11	2085.216			
Corrected Total	10	600.772			

A linear model of the breakthrough

$$Breakthrough = -3.473(\pm 0.668)x - 12.264(\pm 2.672)y + 96.216(\pm 12.358) \quad (6)$$

was also found to be statistically significant at a 95% confidence level, but fit the data slightly less accurately than the quadratic model with an R^2 value of 0.86. Even though there is a large lack of fit observed for all GnP wood filters considered, the surface responses for both the quadratic and linear model clearly indicate that filters tested at lower inlet MB concentrations and flow rates

result in larger breakthrough times. As breakthrough time is indicative of when an adsorbent begins to fail and needs to be regenerated or replaced, these results demonstrate that filters tested at less severe conditions are able to adsorb larger quantities of MB for a longer period of time. The surface response model for the linear regression is also shown in **Figure 13**.

Linear and quadratic models for the cumulative normalized filtrate concentration as a function of inlet MB concentration and flow rate were also determined. The quadratic model

$$Cum\ C_t/C_0 = 0.009\ (\pm 0.001)x^2 - 0.185(\pm 0.031)x - 0.043(\pm 0.020)y^2 + 0.331(\pm 0.142)y + 0.433(\pm 0.265) \quad (7)$$

was found to fit the data more accurately than the linear model with an R^2 value of 0.98. The analysis of variance table for this analysis is shown in **Table 6**. The calculated F value is larger than the critical F value, indicating that this regression is statistically significant at a 95% confidence level. The surface response for this model is given in **Figure 13** and shows that the highest cumulative normalized filtrate concentration is given for GnP filters tested at the highest inlet MB concentration and flow rate.

Table 6. Analysis of variance table for cumulative normalized filtrate concentration as a function of inlet MB concentration and flow rate.

	df	**SS**	**MS**	**F Value**	**Prob>F**
Regression	5	0.12135	0.02427	372.14	2.58E-07
Residual	6	3.91E-04	6.52E-05		
Uncorrected Total	11	0.12174			
Corrected Total	10	0.01582			

A linear model (8) was also found to be statistically significant at a 95% confidence level, but fit the data less accurately than the quadratic model with an R^2 value of 0.73.

$$Cum\ C_t/C_0 = 0.028(\pm 0.007)x + 0.056(\pm 0.027)y - 0.427(\pm 0.138) \quad (8)$$

Even though higher lack of fits are observed at low inlet MB concentrations and flow rates, the regression indicates the same trend as the quadratic model, that higher cumulative normalized filtrate concentrations are observed for GnP filters tested at higher inlet MB concentrations and flow rates. The results from the surface model response for the linear regression are given in **Figure 13**. The results from the surface response analysis results indicate that filters tested at more severe conditions will result in a higher concentration of contaminate in the filtrate, suggesting that they fail more quickly (i.e. shorted breakthrough times) than filters tested at less sever conditions (i.e. lower inlet MB concentrations and flow rates). As cumulative normalized filtrate concentration is inversely related to removal efficiency, filters that resulted in a higher cumulative normalized filtrate concentration also indicates filters with a lower removal efficiency.

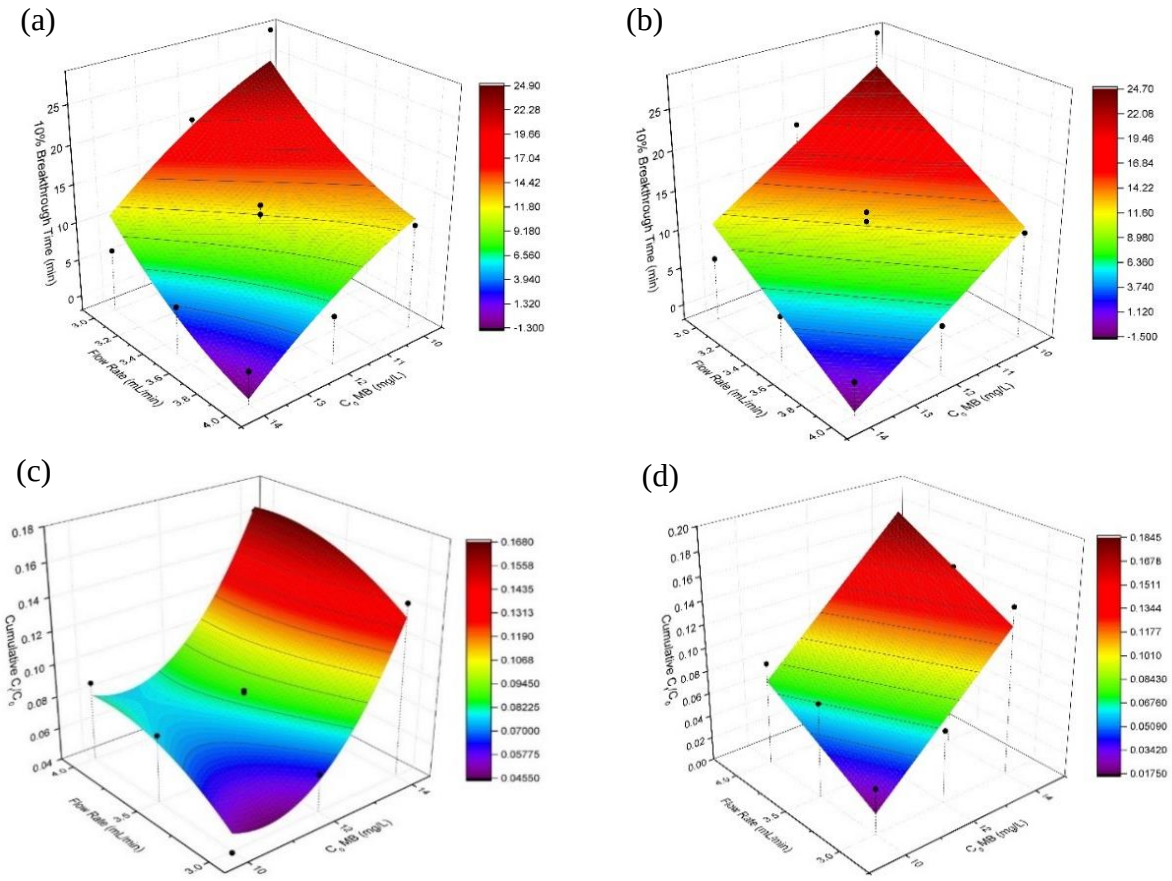

Figure 13. Quadratic (a,c) and linear (b,d) surface response plots for breakthrough time (a,b) and cumulative normalized outlet concentration (c,d) as a function of flow rate and feed concentration of MB.

Regeneration of GnP wood filters

While spent wood filters can be easily burnt after treatment to limit solid waste, the ability to regenerate and reuse the wood filters is attractive from an economic standpoint. In this study solvent regeneration with acetone was employed to desorb the MB from the GnP surface, allowing for the wood filter to be recycled for additional use. After a filter was used in the adsorption of

MB in the continuous column study, the filter was removed and washed with copious amounts of acetone until the UV-Vis spectra of the wash filtrate showed negligible concentrations of MB. Although the wash filtrate was clear, the GnP filters remained visibly blue from the MB that was not able to be desorbed. Some reports suggest that with organic solvents, MB can be desorbed from the surface layer of carbon adsorbents but not from within the mesoporous structure.[74] The MB adsorbed on the surface layer however can be readily desorbed with acetone as it is only weakly bonded to the GnP via physisorption. No chemical bonding has occurred during the adsorption process allowing for the spent filters to be easily regenerated and the MB to be collected for future use if necessary.

Acetone washed GnP filters were retested at the same operating influent conditions (i.e. MB concentration, flow rate) for four additional cycles (cycle 1, 2, 3, 4), for a total of 5 cycles. Cycle 0 indicates the first use of the GnP filter prior to any solvent regeneration and cycles 1 through 4 indicate the times a filter was regenerated and reused since cycle 0. Results showed that when washed with acetone after each cycle, GnP filters were effective at adsorbing MB from aqueous solution for only one additional cycle. The second cycle (cycle 1) achieved almost 100% regeneration efficiency (RE), while the remaining cycles all achieved an RE of approximately 60%. This trend is also represented by the UV-Vis spectra for the normalized filtrate concentration of each cycle, represented in **Figure 14** that shows a significant increase in MB concentration in the filtrate from cycle one to cycles two, three, and four of almost two fold.

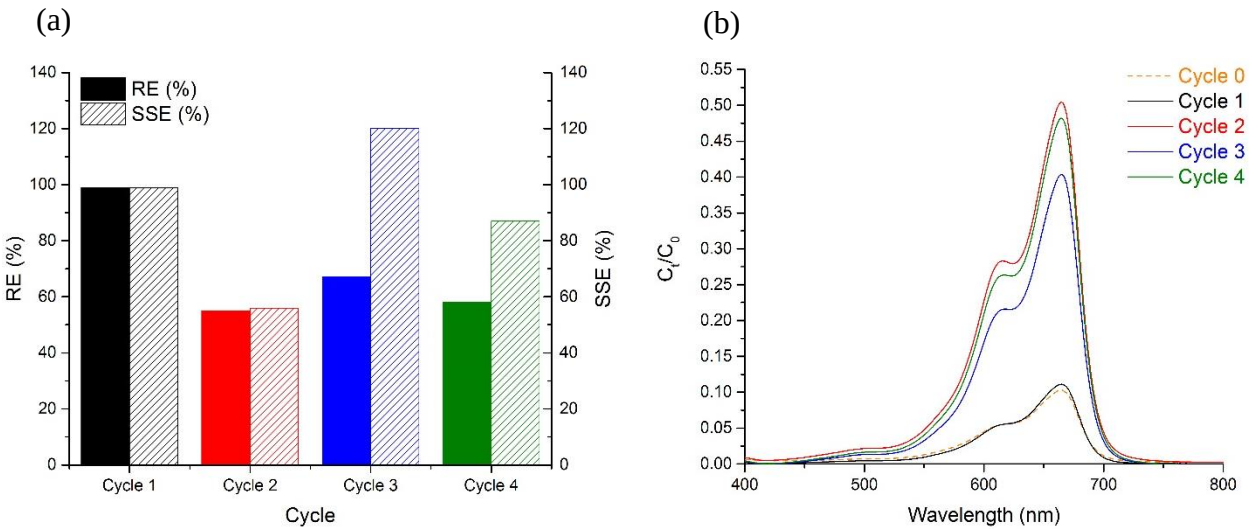

Figure 14. (a) Regeneration and step stripping efficiency for GnP wood filter tested at 14 mg/L MB and 4 mL/min across 4 regeneration cycles. (b) UV-Vis spectra of normalized filtrate concentration for all 5 cycles of GnP wood filter tested at 14 mg/L MB and 4 mL/min.

Although the acetone was able to desorb some of the MB from the GnPs which increased the available surface area for new MB adsorption, the most reasonable explanation for the high RE in cycle one is due to the fact that GnP wood filters were not saturated by MB in the first adsorption trial. In cycle 0, only 100 mL of MB solution was pumped through the GnP filter, resulting in the filter reaching breakthrough but not saturation. After cycle 0 there was still pristine GnP available in addition to the newly regenerated GnP surface area resulting from the acetone wash. Filters were only tested for 100 mL of MB solution, to ensure breakthrough was reached but not saturation, as breakthrough is the point at which a filter would need to be regenerated in a practical application. Although the filters were still adsorbing MB past breakthrough, running a filter through until saturation is impractical as the effluent concentration would be above the recommended environmental and human ingestion levels. As GnP filters were regenerated after breakthrough, it

is reasonable that the second cycle (cycle 1) had almost the same adsorption capacity, as pristine GnP surface area was still available to adsorb MB. After the GnP filter was spent in a second adsorption experiment, it is reasonable to assume that saturation had been reached as the RE dropped to approximately 60% and held relatively steady for the remaining two cycles. The high SSE indicates that after saturation was reached, the solvent regeneration was successful in removing adsorbed MB from the GnP as the efficiency between cycles was relatively high.

CONCLUSION

Complete removal of methylene blue from aqueous solutions by GnP impregnated wood filters was achieved within a broad range of concentrations even at high flow rates. The dispersing ability of lignin to sustainably prepare aqueous suspensions of CNTs is investigated under different conditions and compared to that of typical petroleum-based surfactants. It is demonstrated from UV-vis spectroscopy and optical microscopy that lignin is effective in dispersing and stabilizing aqueous solutions containing CNTs when compared with other anionic and cationic surfactants. Results are described based on the well-established "unzippering" mechanism, and show that there is an optimum dispersant:CNT ratio below or above which the quality of CNT suspension deteriorates. The amphiphilic nature and possibility for π-π interactions with graphitic structures, suggests that the success of lignin in dispersing CNTs can be considered with other graphitic structures such as graphene.

Using lignin as a sustainable surfactant, GnPs were successfully dispersed in aqueous solution and immobilized in basswood templates for use in water treatment. GnP impregnated wood filters were able to efficiently adsorb methylene blue from aqueous solution in a continuous flow system across a wide range of concentrations and flow rates. Kinetic theory models were used to predict

breakthrough curves at different influent conditions and show that GnP impregnated wood filters provide great opportunities for environmental remediation and separation applications.

FUTURE WORK

The results from this work show promise in using GnP-impregnated wood filters for the continuous adsorption of MB from aqueous solutions at a wide variety of inlet concentrations and flow rates. To further improve the functionality and adsorption capacity of these wood filters, and assess the possibility of using these filters under more representative industrial water treatment conditions (i.e. higher flow rates), the GnP loading and wood species will be optimized within a centroid design to achieve the highest MB adsorption as a function of the inlet concentration and flow rate. By varying the GnP loading, and considering the possibility of multiple vacuum impregnation steps to improve the distribution of GnP through wood filters, more surface area can be made available for the adsorption of MB. By testing different wood species with different pore volumes and diameters, higher flow rates more representative of industrial effluents may be modeled to determine the scale up capacity of these GnP-impregnated filters. Based on the changes in adsorption capacity and range of flow rates and concentrations that can be successfully tested, the adsorption capacity for a wide variety of contaminants will also be tested. In a hope to offer a more sustainable adsorbent, GnP wood filters will be tested for adsorbing more organic dyes as well as pesticides typically polluting local water sources as agricultural run-off. The GnP wood filters ability to adsorb contaminants from polluted water collected from water sources near factories and farms in the Pacific Northwest will also be tested to determine the ability of these filters to adsorb pollutants when more than one contaminant is present in solution.

REFERENCES

1 C. J. Vörösmarty, P. B. McIntyre, M. O. Gessner, D. Dudgeon, A. Prusevich, P. Green, S. Glidden, S. E. Bunn, C. A. Sullivan, C. R. Liermann and P. M. Davies, *Nature*, 2010, **467**, 555–561.

2 R. Bos, C. Caudill, J. Chilton, E. M. Douglas, M. Meybeck and D. Prager, in *Ecosystems And Human Well-Being: Current State And Trends*, ME Assessment, Washington, D.C., 2005, vol. 1, pp. 168–197.

3 M. Meybeck, *Philos. Trans. R. Soc. B Biol. Sci.*, 2003, **358**, 1935–1955.

4 F. Chen, A. S. Gong, M. Zhu, G. Chen, S. D. Lacey, F. Jiang, Y. Li, Y. Wang, J. Dai, Y. Yao, J. Song, B. Liu, K. Fu, S. Das and L. Hu, *ACS Nano*, 2017, **11**, 4275–4282.

5 V. Matamoros, C. Arias, H. Brix and J. M. Bayona, *Environ. Sci. Technol.*, 2007, **41**, 8171–8177.

6 A. Cincinelli, T. Martellini, E. Coppini, D. Fibbi and A. Katsoyiannis, *J. Nanosci. Nanotechnol.*, 2015, **15**, 3333–3347.

7 M. T. Yagub, T. K. Sen, S. Afroze and H. M. Ang, *Adv. Colloid Interface Sci.*, 2014, **209**, 172–184.

8 W. L. Ang, A. W. Mohammad, N. Hilal and C. P. Leo, *Desalination*, 2015, **363**, 2–18.

9 L. Huang, J. Chen, T. Gao, M. Zhang, Y. Li, L. Dai, L. Qu and G. Shi, *Adv. Mater.*, 2016, **28**, 8669–8674.

10 S. Dong, J. Feng, M. Fan, Y. Pi, L. Hu, X. Han, M. Liu, J. Sun and J. Sun, *RSC Adv.*, 2015, **5**, 14610–14630.

11 V. K. Gupta, Suhas, I. Tyagi, S. Agarwal, R. Singh, M. Chaudhary, A. Harit and S. Kushwaha, *Glob. J. Environ. Sci. Manag.*, 2016, **2**, 1–10.

12 K. Qian, A. Kumar, H. Zhang, D. Bellmer and R. Huhnke, *Renew. Sustain. Energy Rev.*, 2015, **42**, 1055–1064.

13 S. Hokkanen, A. Bhatnagar and M. Sillanpää, *Water Res.*, 2016, **91**, 156–173.

14 null Thess, null Lee, null Nikolaev, null Dai, null Petit, null Robert, null Xu, null Lee, null Kim, null Rinzler, null Colbert, null Scuseria, null Tomanek, null Fischer and null Smalley, *Science*, 1996, **273**, 483–487.

15 J.-P. Salvetat, G. A. D. Briggs, J.-M. Bonard, R. R. Bacsa, A. J. Kulik, T. Stöckli, N. A. Burnham and L. Forró, *Phys. Rev. Lett.*, 1999, **82**, 944–947.

16 O. V. Kharissova, B. I. Kharisov, V. M. Jiménez-Pérez, B. M. Flores and U. O. Méndez, *RSC Adv.*, 2013, **3**, 22648–22682.

17 S. Kim, Y.-I. Lee, D.-H. Kim, K.-J. Lee, B.-S. Kim, M. Hussain and Y.-H. Choa, *Carbon*, 2013, **51**, 346–354.

18 L. Liu, B. Gao, L. Wu, Y. Sun and Z. Zhou, *Chem. Eng. J.*, 2015, **262**, 1187–1191.

19 M. Sheikholeslam, M. Pritzker and P. Chen, *Carbon*, 2014, **71**, 284–293.

20 Z. Song, J. Dai, S. Zhao, Y. Zhou, F. Su, J. Cui and Y. Yan, *RSC Adv.*, 2013, **4**, 2327–2338.

21 M. Zheng, A. Jagota, E. D. Semke, B. A. Diner, R. S. McLean, S. R. Lustig, R. E. Richardson and N. G. Tassi, *Nat. Mater.*, 2003, **2**, 338–342.

22 R. M. F. Fernandes, B. Abreu, B. Claro, M. Buzaglo, O. Regev, I. Furó and E. F. Marques, *Langmuir*, 2015, **31**, 10955–10965.

23 Y. Bai, D. Lin, F. Wu, Z. Wang and B. Xing, *Chemosphere*, 2010, **79**, 362–367.

24 J. Rausch, R.-C. Zhuang and E. Mäder, *Compos. Part Appl. Sci. Manuf.*, 2010, **41**, 1038–1046.
25 W. H. Duan, Q. Wang and F. Collins, *Chem. Sci.*, 2011, **2**, 1407–1413.
26 R. A. PARHAM and R. L. GRAY, in *The Chemistry of Solid Wood*, American Chemical Society, 1984, vol. 207, pp. 3–56.
27 A. Payen, *Comptes Rendus*, 1838, **7**, 1052–1056.
28 O. Rochez, G. Zorzini, J. Amadou, M. Claes and A. Richel, *J. Mater. Sci.*, 2013, **48**, 4962–4964.
29 P. Estelle, S. Halelfadl and T. Mare, *Int. Commun. Heat Mass Transfer*, 2014, **57**, 8–12.
30 S. M. Goodman, N. Ferguson and A. B. Dichiara, *RSC Adv.*, 2017, **7**, 5488–5496.
31 A. Pénicaud, F. Dragin, G. Pécastaings, M. He and E. Anglaret, *Carbon*, 2014, **67**, 360–367.
32 P. Alafogianni, K. Dassios, S. Farmaki, S. K. Antiohos, T. E. Matikas and N.-M. Barkoula, *Colloids Surf. Physicochem. Eng. Asp.*, 2016, **495**, 118–124.
33 H. Kataura, Y. Kumazawa, Y. Maniwa, I. Umezu, S. Suzuki, Y. Ohtsuka and Y. Achiba, *Synth. Met.*, 1999, **103**, 2555–2558.
34 J.-S. Lauret, C. Voisin, G. Cassabois, C. Delalande, P. Roussignol, O. Jost and L. Capes, *Phys. Rev. Lett.*, 2003, **90**, 057404.
35 S. Attal, R. Thiruvengadathan and O. Regev, *Anal. Chem.*, 2006, **78**, 8098–8104.
36 W. Liu, R. Zhou, D. Zhou, G. Ding, J. M. Soah, C. Y. Yue and X. Lu, *Carbon*, 2015, **83**, 188–197.
37 B. Sohrabi, N. Poorgholami-Bejarpasi and N. Nayeri, *J. Phys. Chem. B*, 2014, **118**, 3094–3103.
38 R. Rastogi, R. Kaushal, S. K. Tripathi, A. L. Sharma, I. Kaur and L. M. Bharadwaj, *J. Colloid Interface Sci.*, 2008, **328**, 421–428.
39 M. S. Strano, V. C. Moore, M. K. Miller, M. J. Allen, E. H. Haroz, C. Kittrell, R. H. Hauge and R. E. Smalley, *J. Nanosci. Nanotechnol.*, 2003, **3**, 81–86.
40 B. Vijayendran, D. Mangara and D. Ensminger, in *Ultrasonics: Data, Equations and Their Practical Uses*, eds. F. B. Stulen and D. Ensminger, CRC Press, Boca Raton, 2008, pp. 323–364.
41 B. Vigolo, A. Pénicaud, C. Coulon, C. Sauder, R. Pailler, C. Journet, P. Bernier and P. Poulin, *Science*, 2000, **290**, 1331–1334.
42 L. Vaisman, H. D. Wagner and G. Marom, *Adv. Colloid Interface Sci.*, 2006, **128**–**130**, 37–46.
43 N.-Y. Teng, I. Dallmeyer and J. F. Kadla, *Ind. Eng. Chem. Res.*, 2013, **52**, 6311–6317.
44 J. Yu, N. Grossiord, C. E. Koning and J. Loos, *Carbon*, 2007, **45**, 618–623.
45 R. Fuge, M. Liebscher, C. Schröfl, S. Oswald, A. Leonhardt, B. Büchner and V. Mechtcherine, *Diam. Relat. Mater.*, 2016, **66**, 126–134.
46 T. Wells, M. Kosa and A. J. Ragauskas, *Ultrason. Sonochem.*, 2013, **20**, 1463–1469.
47 J. G. Duque, A. N. G. Parra-Vasquez, N. Behabtu, M. J. Green, A. L. Higginbotham, B. K. Price, A. D. Leonard, H. K. Schmidt, B. Lounis, J. M. Tour, S. K. Doorn, L. Cognet and M. Pasquali, *ACS Nano*, 2010, **4**, 3063–3072.
48 M. Bystrzejewski, A. Huczko, H. Lange, T. Gemming, B. Büchner and M. H. Rümmeli, *J. Colloid Interface Sci.*, 2010, **345**, 138–142.
49 N. S. Azar and M. Pourfath, *J. Phys. Chem. C*, 2016, **120**, 16804–16814.

50 Y. Bai, J. Gao, C. Wang, R. Zhang and W. Ma, *J. Nanosci. Nanotechnol.*, 2016, **16**, 2239–2245.
51 H. Stewart, M. Golding, L. Matia-Merino, R. Archer and C. Davies, *Food Res. Int.*, 2014, **66**, 93–99.
52 V. K. Thakur, M. K. Thakur, P. Raghavan and M. R. Kessler, *ACS Sustain. Chem. Eng.*, 2014, **2**, 1072–1092.
53 M. Oz, D. E. Lorke and G. A. Petroianu, *Biochem. Pharmacol.*, 2009, **78**, 927–932.
54 M. Kwolek-Mirek and R. Zadrag-Tecza, *FEMS Yeast Res.*, 2014, **14**, 1068–1079.
55 *For. Prod. Wood Sci. Introd.*, , DOI:10.1002/9780470960035.ch5.
56 L. Xu, S. Wang, J. Zhou, H. Deng and R. L. Frost, *Chem. Eng. J.*, 2018, **335**, 450–457.
57 G. Yan, T. Viraraghavan and M. Chen, *Adsorpt. Sci. Technol.*, 2001, **19**, 25–43.
58 A. B. Dichiara, J. Benton-Smith and R. E. Rogers, *Environ. Sci. Nano*, 2014, **1**, 113–116.
59 H. Shi, W. Li, L. Zhong and C. Xu, *Ind. Eng. Chem. Res.*, 2014, **53**, 1108–1118.
60 N. A. Travlou, G. Z. Kyzas, N. K. Lazaridis and E. A. Deliyanni, *Langmuir*, 2013, **29**, 1657–1668.
61 A. C. Ferrari, J. C. Meyer, V. Scardaci, C. Casiraghi, M. Lazzeri, F. Mauri, S. Piscanec, D. Jiang, K. S. Novoselov, S. Roth and A. K. Geim, *Phys. Rev. Lett.*, , DOI:10.1103/PhysRevLett.97.187401.
62 A. B. Dichiara, S. J. Weinstein and R. E. Rogers, *Ind. Eng. Chem. Res.*, 2015, **54**, 8579–8586.
63 K. H. Chu, *Chem. Eng. J.*, 2004, **97**, 233–239.
64 M. Hanbali, H. Holail and H. Hammud, *Green Chem. Lett. Rev.*, 2014, **7**, 342–358.
65 I. Ali, *Sep. Purif. Rev.*, 2014, **43**, 175–205.
66 P. R. Ginimuge and S. D. Jyothi, *J. Anaesthesiol. Clin. Pharmacol.*, 2010, **26**, 517–520.
67 R. Han, Y. Wang, W. Yu, W. Zou, J. Shi and H. Liu, *J. Hazard. Mater.*, 2007, **141**, 713–718.
68 R. Han, Y. Wang, W. Zou, Y. Wang and J. Shi, *J. Hazard. Mater.*, 2007, **145**, 331–335.
69 J.-L. Gong, Y.-L. Zhang, Y. Jiang, G.-M. Zeng, Z.-H. Cui, K. Liu, C.-H. Deng, Q.-Y. Niu, J.-H. Deng and S.-Y. Huan, *Appl. Surf. Sci.*, 2015, **330**, 148–157.
70 N. Mohammed, N. Grishkewich, H. A. Waeijen, R. M. Berry and K. C. Tam, *Carbohydr. Polym.*, 2016, **136**, 1194–1202.
71 L. Sheng, Y. Zhang, F. Tang and S. Liu, *Microporous Mesoporous Mater.*, 2018, **257**, 9–18.
72 G. K. Gill, N. M. Mubarak, S. Nizamuddin, H. S. Al-Salim and J. N. Sahu, *IOP Conf. Ser. Mater. Sci. Eng.*, 2017, **206**, 012081.
73 M. Benallou Benzekri, N. Benderdouche, B. Bestani, N. Douara and L. Duclaux, *J. Mater. Environ. Sci.*, 2018, **9**, 272–284.
74 X. He, K. B. Male, P. N. Nesterenko, D. Brabazon, B. Paull and J. H. T. Luong, *ACS Appl. Mater. Interfaces*, 2013, **5**, 8796–8804.